Paleoceanography and Paleoclimatology

RESEARCH ARTICLE
10.1029/2024PA004860

Astronomical Calibration of the Ocean Anoxic Event 1b and Its Implications for the Cause of Mid-Cretaceous Events: A Multiproxy Record

J. M. F. Ramos[1,2], J. F. Savian[1,3], D. R. Franco[4], M. F. Figueiredo[5], C. G. Leandro[1,4], F. Frontalini[6], R. Coccioni[7], N. Casadei[6], M. Giorgioni[8], P. H. P. C. Vidal[8], E. Yokoyama[8], G. Fazio[4,8], L. Jovane[9], N. Sabatino[10], R. I. F. Trindade[11], and L. R. Tedeschi[12]

[1]Programa de Pós-Graduação em Geociências, Universidade Federal do Rio Grande do Sul, Porto Alegre, Brazil, [2]Petrobras, Exploration - Basin Analysis, Rio de Janeiro, Brazil, [3]Instituto de Geociências, Universidade Federal do Rio Grande do Sul, Porto Alegre, Brazil, [4]Coordenação de Geofísica, Observatório Nacional, Rio de Janeiro, Brazil, [5]Petrobras, Research Center (CENPES), Rio de Janeiro, Brazil, [6]Dipartimento di Scienze Pure e Applicate (DiSPeA), Università degli Studi di Urbino "Carlo Bo", Urbino, Italy, [7]Università degli Studi di Urbino "Carlo Bo", Urbino, Italy, [8]Universidade de Brasília, Instituto de Geociências, Programa de Pós-graduação em Geologia, Brasília, Brazil, [9]Instituto Oceanográfico, Universidade de São Paulo, São Paulo, Brazil, [10]Istituto per lo studio degli Impatti Antropici e Sostenibilità in ambiente marino (IAS-CNR), Palermo, Italy, [11]Instituto de Astronomia, Geofísica e Ciências Atmosféricas, Universidade de São Paulo, São Paulo, Brasil, [12]Petrobras, LIBRA, Rio de Janeiro, Brazil

Abstract The timing and duration of oceanic disturbances linked to Oceanic Anoxic Event (OAE) 1b, as well as the mechanisms driving anoxia and carbon burial during this period, remain subjects of debate. We conducted cyclostratigraphic analyses on magnetic susceptibility (MS) and elemental Ti and Fe series within the upper Aptian-lower Albian interval of the Poggio le Guaine core in the Umbria-Marche Basin, Italy. This interval provides a detailed sedimentary record, supported by variations in magnetic mineral content, Ti, Fe, and significant global shifts in the $\delta^{13}C$ curve. Orbital control of MS, Ti, and Fe suggests a duration of 2.84 Myr for the OAE 1b event. Our chronostratigraphic analysis reveals ages of 114.07 ± 0.12 Ma for 113/Jacob, 113.28 ± 0.12 Ma for Kilian, 112.49 ± 0.12 Ma for the central age of the Monte Nerone cluster, 111.70 ± 0.12 Ma for Urbino, and 111.28 ± 0.12 Ma for Leenhardt sub-events. Stable $\delta^{13}C$ chemostratigraphy correlations enable the transfer of tiepoints across various sedimentary basins. Key features of the carbon isotope curves were identified, named, and dated using astrochronology. Our findings suggest that the organic-rich layers associated with the OAE 1b event exhibit distinct characteristics influenced by several factors, including a warm climate driven by volcanic CO_2 emissions, heightened precipitation, intense weathering, and marine transgressions. These factors amplify orbital forcings on paleoclimate changes, leading to oceanic-atmospheric disturbances that promote deoxygenation and carbon burial during OAE 1b.

Plain Language Summary The causes and consequences of the Cretaceous Oceanic Anoxic Events (OAEs) are a topic of ongoing debate in the literature. One of the most important limitations to answer these questions is the age and duration of these events. The age uncertainty makes the correlations unreliable because the cause-effect is necessary to be time-dependent. In this work, we show the age and duration of the OAE 1b in different records and provide a correlation with orbital forcing and volcanic activity.

Key Points:

- 405-kyr cycles in the magnetic susceptibility and X-ray Fluorescence data indicate an astronomically paced deposition at Poggio le Guaine core during Oceanic Anoxic Event (OAE) 1b
- High-resolution chronostratigraphic study provides a timespan of 2.84 Myr for the OAE 1b
- OAE 1b results from the combination of warm climate, heavy precipitation and intense weathering, acting as amplifiers of orbital forcings

Correspondence to:
J. M. F. Ramos,
j.m.f.ramos@petrobras.com.br

Citation:
Ramos, J. M. F., Savian, J. F., Franco, D. R., Figueiredo, M. F., Leandro, C. G., Frontalini, F., et al. (2024). Astronomical calibration of the ocean anoxic event 1b and its implications for the cause of mid-cretaceous events: A multiproxy record. *Paleoceanography and Paleoclimatology*, *39*, e2024PA004860. https://doi.org/10.1029/2024PA004860

Received 29 JAN 2024
Accepted 16 OCT 2024

Author Contributions:
Conceptualization: J. M. F. Ramos, J. F. Savian, F. Frontalini, R. Coccioni, M. Giorgioni, L. Jovane
Data curation: J. F. Savian
Formal analysis: J. M. F. Ramos, D. R. Franco
Funding acquisition: J. F. Savian
Investigation: J. F. Savian, F. Frontalini, M. Giorgioni, L. Jovane, N. Sabatino
Methodology: J. M. F. Ramos, D. R. Franco
Project administration: J. F. Savian
Resources: J. F. Savian, F. Frontalini, M. Giorgioni, L. Jovane, N. Sabatino
Software: J. M. F. Ramos
Supervision: J. F. Savian
Validation: J. M. F. Ramos, J. F. Savian
Visualization: F. Frontalini, R. Coccioni, M. Giorgioni, L. Jovane

1. Introduction

The Cretaceous greenhouse climate system was punctuated by the occurrence of Oceanic Anoxic Events (OAEs) of regional to global expression (Herrle et al., 2004; Jenkyns, 2010; Leckie et al., 2002; Schlanger & Jenkyns, 1976), commonly characterized by enhanced marine productivity and oxygen deficiency that led to a great accumulation of organic matter at the seafloor and the deposition of black shale layers (Jenkyns, 2010). Arthur et al. (1990) were the first to differentiate the Aptian/Albian anoxic events into OAE 1a and OAE 1b, suggesting sub-events or brief episodes of organic carbon burial linked to marine transgressions. While OAE 1a is defined by a single condensed section deposited over approximately 1 Myr (Leandro et al., 2022), OAE 1b is characterized by a prolonged period of organic carbon burial (Sabatino et al., 2015), including multiple short-duration sub-events (Ait-Itto et al., 2023; Charbonnier et al., 2023; Grippo et al., 2004; Huang et al., 2010; Sabatino et al., 2015).

Writing – original draft: J. M. F. Ramos, R. Coccioni
Writing – review & editing: J. M. F. Ramos, J. F. Savian, D. R. Franco, M. F. Figueiredo, F. Frontalini, R. Coccioni, N. Casadei, M. Giorgioni, P. H. P. C. Vidal, E. Yokoyama, G. Fazio, L. Jovane, N. Sabatino, R. I. F. Trindade, L. R. Tedeschi

The origin of OAE 1b has been associated with global climate warming, with average sea surface temperature between 34°C and 36°C, and high ocean primary productivity (Bottini & Erba, 2018; Bottini et al., 2015; Browning & Watkins, 2008; McAnena et al., 2013; Sabatino et al., 2015), superimposed on influx of continental organic matter (Bodin et al., 2023; Wang et al., 2022). Such high productivity conditions may have been triggered by the emplacements of large igneous provinces (LIPs) such as the Southern Kerguelen (SK), Nauru-Mariana Plateau and Ontong Java Plateau (OJP) (Davidson et al., 2023; Eldholm & Coffin, 2000; Matsumoto et al., 2021, 2022), modifying the paleoclimate and ending the Cold Snap period (McAnena et al., 2013). Micronutrients originating during the emplacement of the LIPs might have fertilized the surface ocean and stimulated the marine primary productivity before and during the OAE 1b interval (e.g., Browning & Watkins, 2008; Leckie et al., 2002).

High concentrations of Hg (Sabatino et al., 2018), combined with continuously increasing trends in strontium and oxygen isotopes, indicate that OAE 1b cannot be characterized as a single event. Instead, it represents a complex, multiphase series of mostly negative $\delta^{13}C$ excursions that span the Aptian/Albian interval and include widespread organic-rich layers. These layers are associated with short-duration episodes of increased marine primary productivity and organic matter preservation (Bodin et al., 2023), with contributions from both continental sources and, occasionally, substantial marine inputs (Bodin et al., 2023; Sabatino et al., 2015).

During OAE 1b, one of the most significant disruptions of the global carbon cycle during the Cretaceous period occurred (Sabatino et al., 2015), and significant efforts have been undertaken to correlate organic-rich layers from OAE 1b across various basins using carbon stable isotopes (Bornemann et al., 2023; Bottini et al., 2015; Fauth et al., 2022; Herrle et al., 2004, 2015). This approach enabled the correlation of the carbonate carbon isotope composite age-calibrated curve (Hinnov & Hilgen, 2012) with the geochemical records from Axel Heiberg Island, Nunavut (Canada), and extended the identification of OAE 1b sub-events to the North Atlantic (Herrle et al., 2015). Herrle et al. (2004) constrained OAE 1b in the Aptian-Albian boundary, a section considerably restricted when compared to the definition by Coccioni et al. (2014) and the GTS2020 (Geologic Time Scale 2020; Gale et al., 2020). Some authors pointed out that Paquier Level is the sole representative of OAE 1b due to its exclusive "paper-shale" characteristic and the heaviest ε^{205} Tl anomaly as a proxy for globally significant ocean deoxygenation (Wang et al., 2022).

The OAE 1b has been estimated in ca. 3 Myr (Coccioni et al., 2014; Leckie et al., 2002; Sabatino et al., 2015, 2018; Trabucho Alexandre et al., 2011), characterized by the occurrence of multiple sub-events as prominent black shale layers observed in the Umbria Marche and Vocontian basins, namely 113/Jacob, Kilian, Urbino/Paquier, and, Leenhardt Levels or equivalent (e.g., Bottini & Erba, 2018; Bottini et al., 2015; Coccioni et al., 2014; Kennedy et al., 2014; Kennedy et al., 2017; Matsumoto et al., 2020). Coccioni et al. (2014) estimated a timespan of 3.8 Myr for OAE 1b in the PLG section (ages inferred from Grippo et al., 2004; Huang et al., 2010; Hinnov & Hilgen, 2012). Ait-Itto et al. (2023), using MS data from two sections of Col de Pré-Guittard (Vocontian Basin, France), determined a duration of 4.03 Myr for the same interval.

The central–western Tethyan pelagic succession in the UMB holds complete and undisturbed records of the Aptian–Albian stages (Coccioni et al., 2012) including the lithological expression of the main organic-rich layers that compose the OAE1b in the Marne a Fucoidi Formation. The presence of the M0r Chron (Savian et al., 2016) and a detailed biostratigraphic zonation (Coccioni et al., 2012, 2014) associated with a dense and systematic multiproxy data sampling allows for the development of a precise age model for the OAE 1b. Through cyclostratigraphy, it is possible to date major fluctuations in the carbon isotope curve and establish correlations between the UMB carbon isotope curve and other carbon isotope curves present in various studies worldwide.

In this paper, we utilize advanced cyclostratigraphic methods to detect orbital cycles within the interval covering the OAE 1b of the PLG core (Coccioni et al., 2012; Leandro et al., 2022; Matsumoto et al., 2021, 2022; Savian et al., 2016). We utilized a comprehensive data set comprising MS data, XRF (X-ray Fluorescence) measurements, and stable isotope $\delta^{13}C$ correlations. Our new study offers insights into the Aptian/Albian transition and a comprehensive analysis of the OAE 1b event, redefining its duration and exploring the factors driving anoxia and carbon burial during this period. We use some of the most advanced techniques for recognition and characterization of orbital cycles and sedimentation rates. The objectives of this work are as follows: (a) to define the duration of the OAE 1b event and its sub-events; (b) to provide a carbon-isotope correlation framework for the existing absolutes dating through correlations between markers in different carbon isotope curves; and (c) to discuss (in geological time) the paleoclimate and astronomical forcings causing carbon burial during the period of

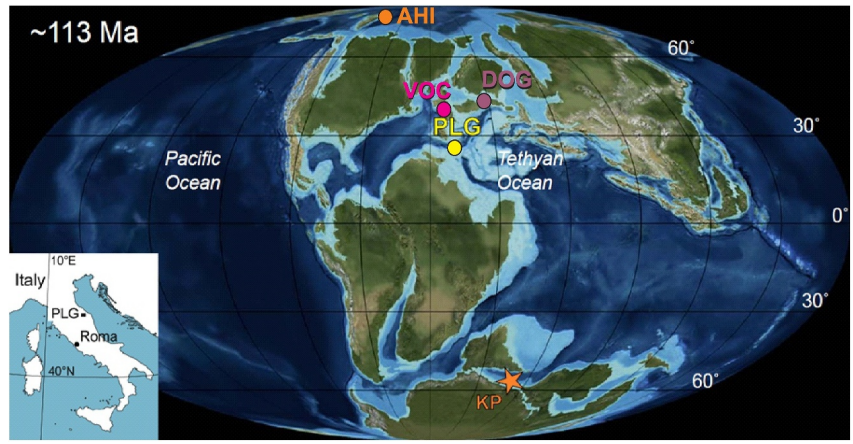

Figure 1. Paleogeographic reconstruction for the Aptian-Albian transition at ~113 Ma (modified after Sabatino et al., 2018) showing the location of the Poggio le Guaine, Vocontian Basin (VOC), Dolgen 3 core (DOG), Axel Heilberg Island, and of the Kerguelen Plateau (KP).

anoxia. The possibility of joint observation among Fe, Ti, and MS data allows for new insights into the cause-and-effect relationship between paleoclimatic response to orbital forcings and the deposition of black shale levels. Additionally, converting the carbon isotope curve to the time domain, including its excursions and trends in the PLG, allows the correlation of different sedimentary basins also in the geological time domain and provides information about sedimentation rates, possible unconformities, and/or condensed sections.

2. Materials and Methods

2.1. Poggio le Guaine Records: Section and Core

The Cretaceous pelagic succession of the UMB was deposited in a complex geological setting along the continental margin of the Apulian block, which was moving along with Africa toward northern Europe at that time (Channell et al., 1979). After decades of research, the Aptian–Albian pelagic succession of the UMB has become a classic reference record for regional to global scale paleoenvironmental studies on OAEs (Coccioni et al., 2014; Leandro et al., 2022; Matsumoto et al., 2020, 2021, 2022; Sabatino et al., 2015, 2018; Savian et al., 2016). This succession was deposited well above the calcite compensation depth (CCD) at middle to lower bathyal depths (1,000–1,500 m) and at a paleolatitude of approximately 20°N, on the southwestern margin of the Tethyan Ocean (Arthur & Premoli Silva, 1982; Coccioni et al., 1987, 1989, 1990, 1992; Savian et al., 2016).

The Aptian-Albian pelagic succession of the UMB extends from the upper part of the Maiolica Fm (Tithonian to lower Aptian) to the lower part of the Scaglia Bianca Formation (upper Albian to lower Turonian) and includes the Marne a Fucoidi Formation in between. The upper part of the Maiolica Fm is represented by centimeter thick beds of white to gray limestone interspersed with black shales. The lower part of the Scaglia Bianca Formation is characterized by centimeter thick beds of yellowish-gray limestones with reddish limestones and an interval with centimeter thick black shale layers in the lower part (Pialli Level; Coccioni, 2001), which is part of the sedimentary expression of the lower part of OAE 1d. The PLG section outcrops in the eastern portion of Monte Nerone (Figure 1; latitude 43°32′29.06″ N, longitude 12°34′51.09″ E). Lithologies comprises pale reddish brown to dark reddish brown and pale olive to greyish olive argillaceous limestones and calcareous marlstones, marlstones, slightly calcareous mudstones to argillaceous mudstones with several cyclically alternating organic–rich black shales and mudstones (Coccioni et al., 2014).

Several organic-rich horizons (Figure 2) representing the regional expression of the global OAE 1b have been identified (Coccioni, 1996; Coccioni et al., 1990, 2012, 2014; Leckie et al., 2002; Matsumoto et al., 2020, 2022; Petrizzo et al., 2012; Sabatino et al., 2015, 2018; Trabucho Alexandre et al., 2011) and spanned from the upper Aptian to lower Albian (~114 and 109 Ma) (e.g., Coccioni et al., 2014). These events include the upper Aptian 113/Jacob, the lowermost Albian Kilian, the Albian Monte Nerone cluster, the Albian Urbino/Paquier, and the Albian Leenhardt organic-rich marker beds (Coccioni et al., 2014; Matsumoto et al., 2020, 2022; Sabatino et al., 2015, 2018).

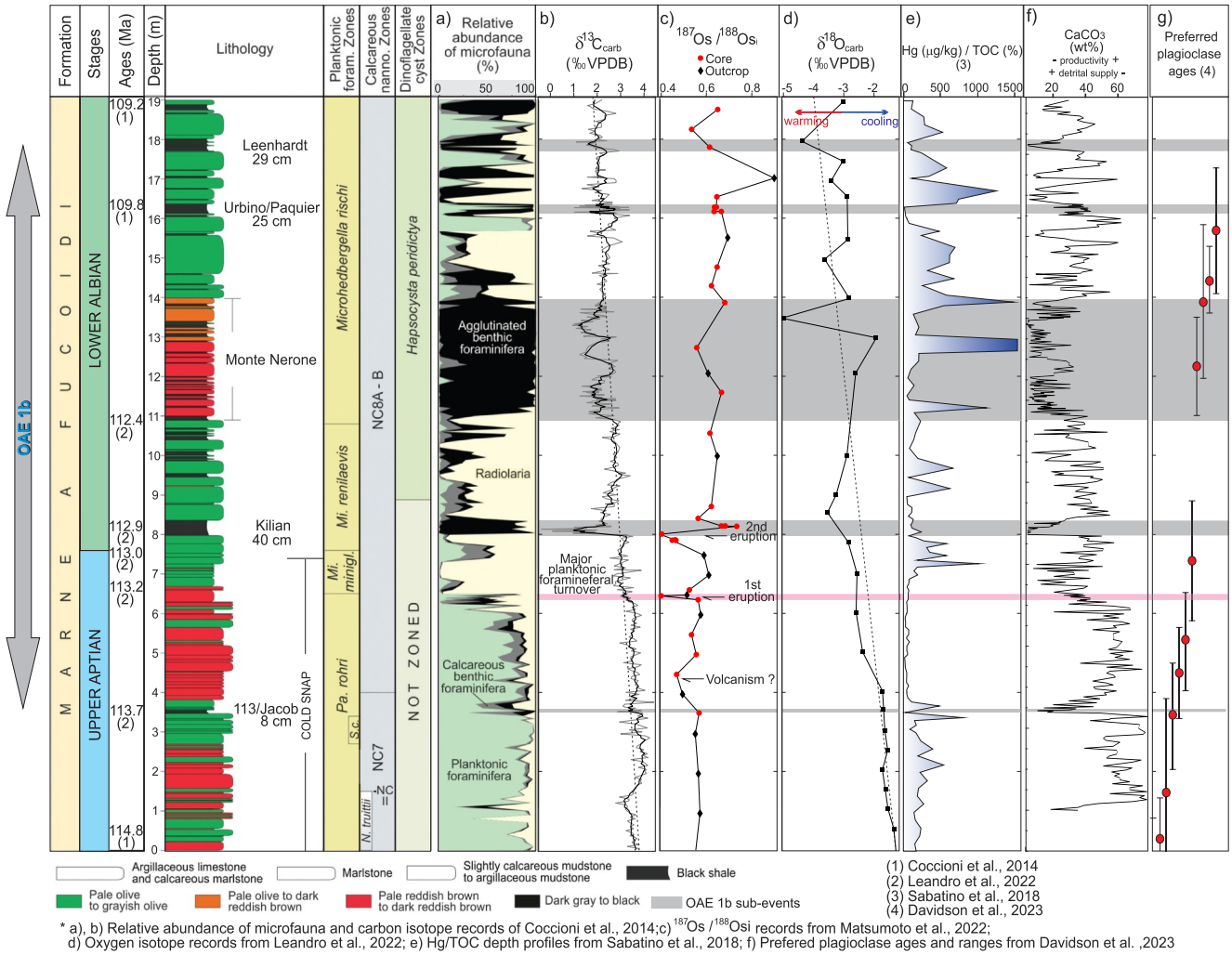

* a), b) Relative abundance of microfauna and carbon isotope records of Coccioni et al., 2014;c) $^{187}Os/^{188}Osi$ records from Matsumoto et al., 2022;
d) Oxygen isotope records from Leandro et al., 2022; e) Hg/TOC depth profiles from Sabatino et al., 2018; f) Prefered plagioclase ages and ranges from Davidson et al. ,2023

Figure 2. Characterization of Oceanic Anoxic Event 1b and Aptian-Albian transition at Poggio le Guaine section plotted against (a) the relative abundance of microfauna from Coccioni et al. (2014); (b) $\delta^{13}C_{carb}$ data from Coccioni et al. (2014); (c) $^{187}Os/^{188}Os$ isotopic record from Matsumoto et al. (2020); (d), $\delta^{18}O_{carb}$ data from Leandro et al. (2022); (e) Hg/TOC depth profiles from Sabatino et al. (2018); (f) $CaCO_3$ from Coccioni et al. (2014); (g) preferred plagioclase ages from Davidson et al. (2023). The diamond and asterisk mark highest occurrence of *Pseudoplanomalina cheniourensis* and the lowest occurrence of *Pleurostomella subnodosa*, respectively. Vertical scale according to Coccioni et al., 2014. Key to planktonic and calcareous nannofossil abbreviations: *Pa.* = *Paraticinella*, *Mi.* = *Microhedbergella*, *minigl.* = *miniglobularis*, *S.* = *Shackoina*, *c.* = *cepedai*, *N.* = *Nannoconus*.

The most comprehensive cyclostratigraphic evaluation of a high-resolution multiproxy data set from the Poggio le Guaine (PLG) core was conducted by Leandro et al. (2022), providing new constraints for the Aptian climato-chronostratigraphic framework. According to the inferred ages of Leandro et al. (2022), the Aptian-Albian boundary is set at 113.0 Ma at PLG core in correspondence of the First Occurrence (FO) of *Microhedbergella renilaevis (M. renilaevis)*, an age very similar to that attributed to Vöhrum's tuff (Selby et al., 2009). High-resolution planktonic foraminiferal and calcareous nannofossil biostratigraphy, microfaunal (i.e., benthic and planktonic foraminifera, and radiolaria) assemblages, in combination with a detailed carbon and oxygen isotope record of the PLG section (Coccioni et al., 2014), associated with Os isotopic record (Matsumoto et al., 2020) and new preferred plagioclase ages (Davidson et al., 2023) were used to characterize OAE 1b in this work (Figure 2). The "red" layers named as CORBs (*Cretaceous Oceanic Red Beds*) (Wang et al., 2009) appear related with new preferred plagioclase ages from OJP volcanism (Davidson et al., 2023) and show an intrinsic relationship with changes in the relative abundance of microfauna (Coccioni et al., 2014) reflecting regional paleoenvironmental conditions.

The GSSP of Aptian/Albian boundary (i.e., the base of the Albian Stage) has been defined at Col de Pré-Guittard (Vocontian Basin, southeast France) and corresponds to FO of the planktonic foraminifer *Microhedbergella miniglobularis (M. miniglobularis)* within the thin organic rich Niveau Kilian Level (Gale et al., 2020; Kennedy et al., 2017) coinciding with a negative carbon isotope excursion. The drop in the abundance of planktic foraminifera relative to benthic species that globally occur in deep-sea records (Huber & Leckie, 2011) is also shown at the PLG section across the Aptian/Albian boundary (Coccioni et al., 2014). The abrupt planktonic foraminiferal turnover across the Aptian–Albian boundary during OAE 1b can be ascribed to enhanced ocean acidification caused by the massive release of volcanic CO_2 (Matsumoto et al., 2020). Abrupt Os isotopic shift to unradiogenic values and elevated Hg concentrations suggest multiple submarine volcanic events that correlate with new plagioclase ages, further increasing the relationship between the OJP and the paleoenvironmental changes during OAE 1b (Davidson et al., 2023; Matsumoto et al., 2020; Sabatino et al., 2018).

The absence of physical evidence of unconformable surfaces (Coccioni et al., 2014), the deposition above CCD (Coccioni et al., 1990), the presence of the M0r reversal Chron as main tiepoint for the Aptian base (Savian et al., 2016) make the PLG a suitable reference record, ideal to test cyclostratigraphic techniques and dating major geological events (e.g., isotopes excursions, bioevents, volcanic pulses). Also, the clear orbital forcing response of several Tethyan records (Charbonnier et al., 2023; Grippo et al., 2004; Huang et al., 2010; Leandro et al., 2022; Tateo et al., 2000) have stimulated this new cyclostratigraphic evaluation. This study combines the existing array of data within the context of the PLG section ($CaCO_3$, $\delta^{13}C$, $\delta^{18}O$, $^{187}Os^{186}Os$, Hg; Coccioni et al., 2014; Sabatino et al., 2018; Matsumoto et al., 2020) with new data acquired from the PLG core (MS, XRF, and $\delta^{13}C$).

2.2. Sampling

The drilling site of the PLG core is located 400 m northwest of the PLG section (Coccioni et al., 2012) and has a straightforward correlation with it (Figure 3) through its organic-rich marker beds and black shale levels, allowing for direct correlation between them. The PLG core was drilled in 2010 and designed to provide a high-resolution reference record for the Aptian-Albian interval. Once in the laboratory, the core was split into two halves along the dip line of the bedding. The left side (archived) of the core was plastic coated, packed, and housed at the University of Urbino (Italy). The right side (working half) of the core was cut into four parts, comprising two lateral sections, a bottom section, and the center of the split core (Savian et al., 2016). The center of the split core and bottom sections were cut in discrete cubic samples from the center of the split core sections in cubes of ~8 cm^3 for environmental magnetism analyses. Overall, we collected 3,437 paleomagnetic samples with an averaging spacing of ca. 3 cm, from 0 to 95 m along the PLG core. The weight of each sample was determined for subsequent mass normalization of magnetic properties. The same samples were also used for isotopic analyses. For this study, we only focused on OAE 1b interval from 52 to 70 m resulting in 639 paleomagnetic samples with an averaging spacing of ca. 2.8 cm. The calcium carbonate ($CaCO_3$) was compiled from Sabatino et al. (2015).

2.3. Magnetic Susceptibility

The MS (χ, mass specific normalized low field magnetic susceptibility) measurements were carried out at the Paleomagnetic Laboratory of the University of São Paulo (USPMag, Brazil). Frequency dependence of the MS was measured in a total of 639 samples before remanence measurements. Measurements of the MS were made on an MFK1-FA Multi-Function Kappabridge (Pokorný et al., 2006) at three operating frequencies (976, 3904 and 15616 Hz) in a field of 200 A/m. For this work, we only used the 976 Hz frequency for the cyclostratigraphic study.

2.4. XRF Measurements

The XRF data were collected using a S1 Titan handheld XRF spectrometer, with a slit of 1 cm parallel and 0.7 cm perpendicular to the core length, and a sampling rate of 5 cm. Analyses were made at the University of Urbino (Italy), conducted on the PLG core. A wide range of chemical elements was identified with two tube voltage settings: at 10 and 50 kV, each with five replicates and 30s acquisition time. After the measurement, anomalous values due to alteration of the core surfaces or analytical issues were removed from the series and the data were normalized respect to the total average of the series. Series of Ti and Fe were selected for cyclostratigraphic analysis and for paleoenvironmental interpretations. Approximately 561 data points were measured to construct the XRF-derived elemental time Ti and Fe series.

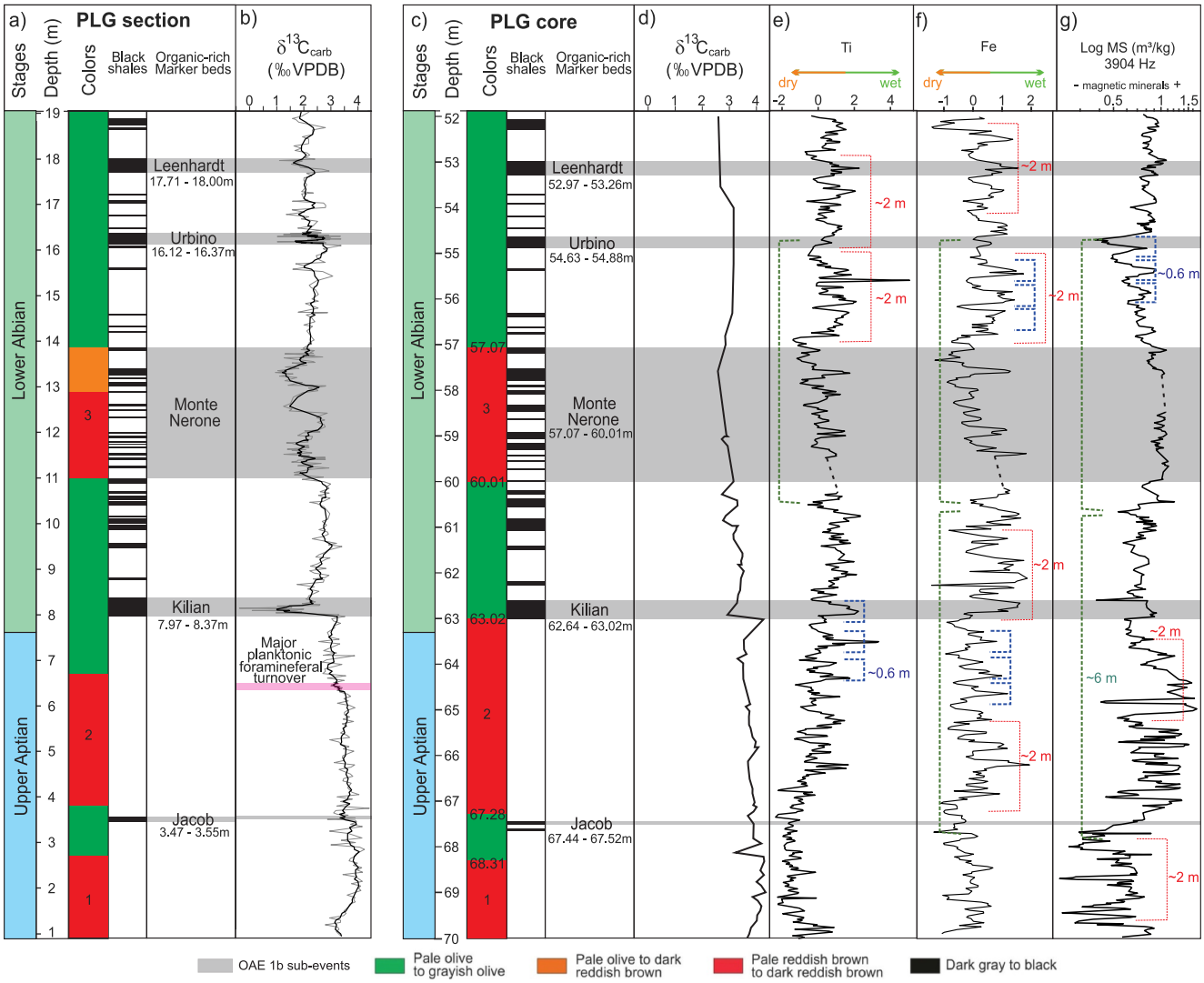

Figure 3. Correlation between the Poggio le Guaine (PLG) section (left, Coccioni et al., 2012) and PLG core (right, Coccioni et al., 2014) through its organic-rich marker beds and black shale levels: (a) PLG section colors, black shale levels and organic-rich marker beds. Vertical scale from Coccioni et al. (2014); (b) $\delta^{13}C_{carb}$ data from Coccioni et al. (2014); (c) PLG core colors, black shale levels (ordered in ascending numbers from the base to the top) and organic-rich marker beds. Vertical scale from Coccioni et al. (2012); (d) $\delta^{13}C_{carb}$ data, this study; (d) Ti content; (e) Fe content; (e) Log MS. Three cyclic patterns are highlighted by dashed lines.

2.5. Stable Carbon Isotope

Carbon ($\delta^{13}C$) stable isotope analyses were performed in the carbonate fraction at the University of Oxford (UK). A total of 106 bulk-rock samples were collected under different spacings, resulting in an average spacing of ~16.9 cm and used to characterize the OEA 1b event. A rotary drill was used to obtain powder from the cubes used for magnetostratigraphic measurements. During sampling, veins containing diagenetic carbonate were avoided. A total of eight triplicates and three duplicates of the same depth were used to evaluate the reproducibility of the isotopic data. The powders of 95 samples were analyzed using a VG Isogas Prism II mass spectrometer with an online VG Isocarb common acid-bath preparation system at University of Oxford (UK).

All these samples were cleaned using acetone [$(CH_3)2CO$] and dried at 60°C for at least 30 min. The powders of 11 samples were analyzed using a Gas Bench II carbonate device coupled to a Thermo Scientific Delta V mass spectrometer. Samples were reacted with purified phosphoric acid (H_3PO_4) at 70–90°C in all instruments. The calibration was undertaken using the Oxford in-house Carrara marble standard (NOCZ) and NBS-19 (TS-Limestone). Data are reported relative to the Vienna Pee Dee Belemnite (VPDB) scale. The reproducibility of

replicated standards (1σ) was <0.09‰ for $\delta^{13}C$. The maximum difference between triplicate and duplicate samples from the same depth were 0.31‰ for $\delta^{13}C$.

2.6. Cyclostratigraphic Analysis

Cyclostratigraphic analyses on MS and XRF-derived Ti and Fe records were conducted using *Acycle* software (Li et al., 2019), version 2.4.1, and the Astrochron package Version 1.2 (Meyers, 2014). While the MS data set exhibited a non-stationary variance and was log-transformed to stabilize it, this pattern was not present in the Fe and Ti data sets, so log-transformation was not needed. All series were then linearly interpolated each 2 cm, which is the average spacing of the Fe, Ti and MS series. Prior to the spectral analysis, all data sets were detrended using the Loess method with a of 35% sliding window. Spectral analysis was conducted by the prolate multitaper spectral estimator (MTM, Thomson, 1982) against a robust first-order autoregressive red-noise null model (Mann & Lees, 1996). Solely the spectral peaks which exceed a threshold of 95% confidence level (CL) for both spectral analysis and the F-test (Meyers & Sageman, 2007) were considered in our work. The persistence and/or transience of the astronomical signals along the series were assessed by means of Evolutive Harmonic Analysis (EHA) (Meyers et al., 2001), as well as to provide indications of fluctuations in the sedimentation accumulation rate (SAR).

We considered potential astronomical frequencies that may correspond to those expected for the Tethyan pelagic succession in the UMB at Aptian–Albian times based on the La2004 astronomical solution (Laskar et al., 2004), similarly to the performed in previous works (e.g., Grippo et al., 2004; Huang et al., 2010; Leandro et al., 2022). Regarding the high stability of ∼405 kyr long-eccentricity over geological times and hence its suitably as a metronome over the Phanerozoic (Laskar, 2020), we isolated the interpreted 405 kyr long-eccentricity sinusoidal component from the MS data set by a dynamic filtering process (available in the *Acycle* package). It allowed us to perform an astronomical tuning by correlating the 405 kyr component of the MS series with the La2004 g_2–g_5 target curve and the depth-to-time domain calibration of the MS and $\delta^{13}C_{carb}$ data. We used as tiepoints for the astronomical tuning the $^{206}Pb/^{238}U$ absolute age of the basal Albian for the Schwicheldt Ton Member, Gault Formation, Vöhrum, Germany (Bornemann et al., 2023; Selby et al., 2009) and the U-Pb age (111.74 ± 0.26 Ma, using bentonite zircons) of the Invincible Point Member, Christopher Formation (Herrle et al., 2015)—which were further compared with the ages of Jacob and Kilian Levels provided by Leandro et al. (2022). Changes in the SAR throughout the succession were evaluated by COCO/eCOCO (Li et al., 2018) and TimeOpt/eTimeOpt (Meyers, 2015, 2019) analyses. In order to recover the phase of MS data related to the astronomical solutions, we also conducted a time-scale optimization analysis (TimeOpt; Meyers, 2015). Furthermore, we performed the Average Spectral Misfit (ASM) (Meyers & Sageman, 2007) to identify statistically significant harmonic components and estimate uncertainties of the astronomical signals within the stratigraphic data series, providing an explicit statistical test for rejecting the null hypothesis.

3. Results

3.1. XRF

After normalization by mean and operation of dividing by the standard deviation, Ti normalized values vary from −2.4 to 5 and Fe from −2 to 3, and their variations could be used as proxies of detrital supply (Herbert & Fischer, 1986) and continental runoff (Arz et al., 1998). A more distinct linear trend is observed in the Ti series compared to the Fe series; however, both data sets exhibit a similar pattern. It is possible to observe the presence of at least three cyclic patterns (highlighted by dashed lines, Figure 3) with different wavelengths. The green dashed line represents the cyclic pattern with the longest wavelength, spanning about 5 m, and serves to modulate the other cycles. Across the studied section, the intermediate cycle (red dashed line) has a more pervasive presence with a characteristic wavelength of about 2 m. This cycle, in its turn, influences the adjacent 0.5 m cycle, particularly noticeable in thicker black shale strata (blue dashed line).

In general, black shale levels can be associated with positive peaks in Ti and Fe content (e.g., the Kilian and Leenhardt Levels; see Figures 3e and 3f). However, some occurrences of black shale are characterized by negative peaks, while others show an inverse correlation between Ti and Fe contents (see Figures 3e and 3f). Furthermore, certain levels, such as the black shale associated with the Urbino Level, exhibit no discernible relationship between these elements.

3.2. Magnetic Susceptibility

The MS underlies the amount of magnetic minerals (e.g., Liu et al., 2020) and could also be used as a proxy for detrital input throughout Fe minerals. Our MS record (mean of $\chi = 7.7 \times 10^{-8}$ m^3/kg) exhibited three stratigraphic long-term quasiperiodicies (~6 m) that would be partly associated with microfaunal changes (Figure 3g). The 70–67.5 m basal interval is characterized by the lowest values of MS that might be ascribed to low sedimentary input, which is followed by a 5-m-thick interval marked by the highest values MS and reddish lithologies between 113/Jacob and below Kilian Levels. The Monte Nerone cluster (57.07–60.01 m in PLG core; Coccioni et al., 2012) is marked by relatively stable MS values. Such lithostratigraphic interval is also characterized by a cyclic pair of black shales and mudstones with the dominance of agglutinated foraminifera. The upper part of the studied interval is quite different from the lower one. Short oscillations (~0.6 m wavelengths) were also noticed, most of the time in phase with Ti and Fe contents. The Urbino/Paquier black shale (54.63–54.88 m in PLG core) corresponds to a prominent negative short-term variation of MS.

3.3. Stable Carbon Isotope

After carefully assessing the sampling/resolution of the PLG core in relation to the PLG section, it was decided to transfer the stratigraphic elevations of the Carbon isotope data series from the PLG section to the PLG core using the base of the negative excursion of the Kilian Level as the datum (Figure 3). Furthermore, the black shale levels and sediment colors enable us to conduct a concise transposition of the stratigraphic elevations from the Carbon isotope data series of the PLG section to the PLG core. It is worth noting that in despite the successful transposition, it was not utilized in the cyclostratigraphic spectral analyses.

3.4. $\delta^{13}C$ Chemostratigraphic Correlation

Since there are no available radiometric ages for the Aptian-Albian interval of the PLG core, it was necessary to transpose tiepoints between different places though correlations based on stable $\delta^{13}C$ chemostratigraphy. Even in distinct geological contexts (different depositional environments), the shapes of the $\delta^{13}C$ curves could be correlated to each other (Bodin et al., 2023) and use them as global tiepoints. These correlations aim to reconcile the $\delta^{13}C$ markers with numerical ages. We correlate carbon isotope stages (CIS) (Coccioni et al., 2014; Herrle et al., 2004; Leandro et al., 2022) and highlight prominent features, represented by excursions, peaks, troughs, and breaks in the long-term behavior of the carbon isotope curves (Figure 4 and Table 1).

Using the sequence of letters from the Greek alphabet, from **α** to **ο**, where: ***k*** is the onset of the Killian excursion and F.O. of *M. renilaevis*; **λ** is the Kilian prominent negative carbon excursion; **μ** is the end of this excursion, coincident the Vöhrum tuff horizon (Bornemann et al., 2023), and the **ο** marker (positioned by correlation in ~54 m, at PLG) is stratigraphically placed very close to absolute U-Pb 111.74 ± 0.26 Ma age estimation (bentonite zircons) from Herrle et al. (2015) (Table 1 and Figure 4c). We also used stages definitions, foraminiferal and nannofossil events (Bornemann et al., 2023; Coccioni et al., 2014; Herrle et al., 2004, 2015; Leandro et al., 2022) to correlate CIS intervals, and match Glendonite beds (Herrle et al., 2015) as an effect of Cold Snap interval to reinforce our age's transposition. The ammonite zones, even with the possibility of occurrence in a limited region (Kennedy et al., 2014), have also been included in our correlation's framework. We used transposed ages as anchors at the beginning of tuning process, and later it was released during direct correlation between MS-based 405-kyr sinusoidal component.

The top of OAE 1a event is characterized by a positive excursion name here by **α** (Figure 4) expressed as a higher $\delta^{13}C$ peak at the base of a high values plateau in the *Leupoldina cabri* (*L. cabri*) foraminiferal zone. Positive long-term C-isotope trend is interrupted by a negative excursion (lower peak) detectable mainly in the Tethyan realm, associated with *Niveau Blanc* (Charbonnier et al., 2023; Herrle et al., 2004) and Wezel Level (Leandro et al., 2022; Matsumoto et al., 2020), pointed as **β** (~117.9 Ma; Leandro et al., 2022). The upper part of the positive interval described as Ap 7 C-isotope stage (Herrle et al., 2004) is followed by a huge negative excursion that coincides with *Globigerinelloides ferreolensis*/*Globigerinelloides algerianus* biostratigraphic zones boundary. The most $\delta^{13}C$ positive peak in *Globigerinelloides ferreolensis* at the end of high values plateau was named **γ**, a higher peak at end of a high values plateau.

The **δ** marker is clearly visible around all regions of Earth, associated with *NCC2* (Charbonnier et al., 2023; Herrle et al., 2004) and Noir Level (Charbonnier et al., 2023; Gale et al., 2020), also recognized by the long-term

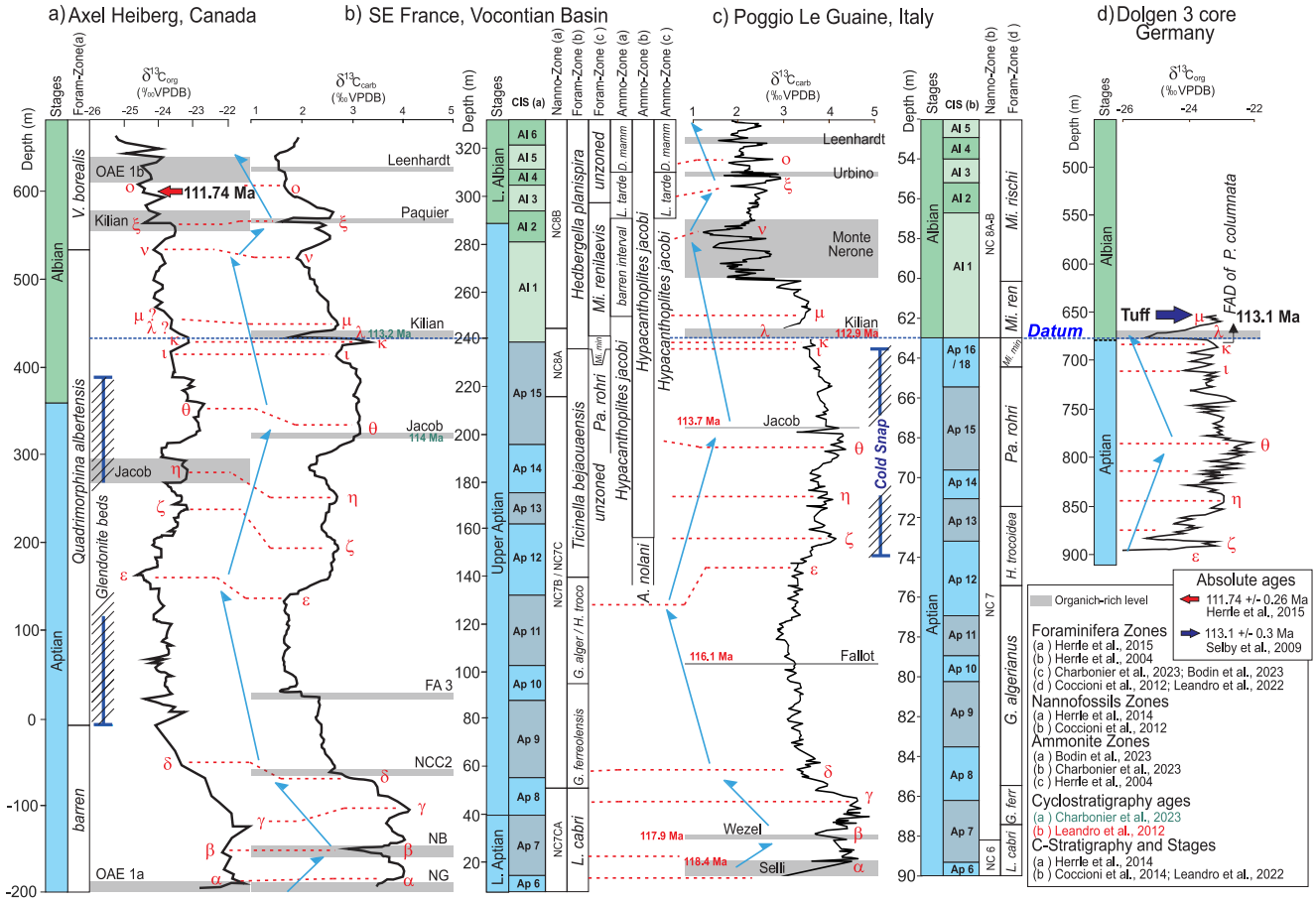

Figure 4. Correlation of C-isotope records showing the major patterns and C-marks of: (a) Axel Heiberg Island, Canada; (b) Vocontian Basin, France; (c) Poggio le Guaine, Italy; (d) Dolgen-3 core, Germany. Absolute ages and biozones are detailed in the legend. Gray shadings represent organic-rich marker beds. Modified from Leandro et al. (2022), Herrle et al. (2015), Coccioni et al. (2014), Herrle et al. (2010), Bodin et al. (2023), Charbonnier et al. (2023), Nebe (1999), and Bornemann et al. (2023). Light blue arrows indicate the long-term trends.

inflection change in the carbon isotope curve, as a lower $\delta^{13}C$ shift above a high values plateau at the base of the *Globigerinelloides algerianus* (*G. algerianus)* foraminiferal zone. Except for the (relatively small) negative excursion associated with the Fallot Level or FA 3, from this point onward, the curves show a gradual decrease in $\delta^{13}C$ values until the **ε** marker, where a significant shift in curve behavior occurs, and values begin to increase. These markers end a low $\delta^{13}C$ values plateau and begins an increasing trend in the *Hedbergella trocoidea (H. trocoidea)* foraminiferal zone.

The **ε** marker is related to the onset of a C-isotope positive shift, which marks the beginning of a long interval with relatively high $\delta^{13}C$ values, in which the **ζ**, **η** and **θ** markers could be defined. This interval is related to a cooler period called Cold Snap in the Tethyan Ocean (Bodin et al., 2023; Bottini et al., 2015; McAnena et al., 2013). The **ζ** marker is characterized as the end of a $\delta^{13}C$ increasing trend in the *H. trocoidea* foraminiferal zone, while the **η** marker is a relatively higher $\delta^{13}C$ peak within a high values plateau across the *H. trocoidea*/*Paraticinella rohri* foraminiferal zones.

Herrle et al. (2015) positioned the Jacob Level at Axel Heiberg (~300 m; Figure 4a) below the position where the long-term trend of carbon isotope curve inflects (**η** marker). This feature is related to Ap 13 C-isotope stage in the Vocontian Basin, but Charbonnier et al. (2023) dated the Jacob Level as a 114 Ma, within the Ap 15 C-isotope stage. Leandro et al. (2022) dated the Jacob event at 113.7 Ma that is characterized as a $\delta^{13}C$ negative excursion (Figure 4c).

The **θ** marker is the highest $\delta^{13}C$ peak at the top of a high values plateau in the *Paraticinella rohri (Pa. rohri)* foraminiferal zone. Above this marker, the C-isotope curves slightly decrease and are punctuated by a short-term

Table 1
Characteristics and Positioning of C-Markers Into Chemostratigraphic Stages in Poggio le Guaine

Marker	CIS	F.Z.	N.Z.	Characteristics
α	Ap 6-7	*L. cabri*	NC 6	Higher $\delta^{13}C$ peak at the base of a high values plateau in the *L. cabri* foraminiferal zone.
β	Ap 7	*L. cabri*	NC 7	Lower $\delta^{13}C$ peak within a high values plateau in the in *L. cabri* foraminiferal zone.
γ	Ap 7	*G. ferr*	NC 7	Higher $\delta^{13}C$ peak at end of a high values plateau in the *G. ferr.* foraminiferal zone.
δ	Ap 8	*G. alger*	NC 7	Lower $\delta^{13}C$ shift above a high values plateau at the base of the *G. alger.* foraminiferal zone.
ε	Ap 11-12	*H. troc*	NC 7	End of a low $\delta^{13}C$ values plateau and beginning of increasing trend in the *H. trocoidea* foraminiferal zone
ζ	Ap 12	*H. troc*	NC 7	End of a $\delta^{13}C$ increasing trend in the *H. trocoidea* foraminiferal zone
η	Ap 13	*P.rohri*	NC 7	Relatively higher $\delta^{13}C$ peak within a high values plateau across the *H. troc./Pa. rohri* foraminiferal zones.
θ	Ap 15	*P.rohri*	NC 7	Higher $\delta^{13}C$ peak at the top of a high values plateau in the *Pa. rohri* foraminiferal zone.
ι	Ap 15–Al1	*Mi.min*	NC 8A-B	Lower $\delta^{13}C$ peak at the top of a decreasing trend in the *Mi. min.* foraminiferal zone.
κ	Al1	*Mi.ren*	NC 8A-B	Abrupt higher $\delta^{13}C$ peakin the *Mi. ren.* foraminiferal zone, preceding the Kilian negative excursion.
λ	Al1	*Mi.ren*	NC 8A-B	Abrupt lower $\delta^{13}C$ peak in the *Mi. ren.* foraminiferal zone, associated with the Kilian event.
μ	Al1	*Mi.ren*	NC 8A-B	Positive $\delta^{13}C$ shift in the *Mi. ren.* forabminiferal zone, above the Kilian negative peak.
υ	Al1	*Mi.rischi*	NC 8A-B	Top of a $\delta^{13}C$ decreasing trend in the *Mi. rischi* foraminiferal zone.
ξ	Al 2-3	*Mi.rischi*	NC 8A-B	Top of a $\delta^{13}C$ increasing trend in the *Mi. rischi/planispira* foraminiferal zone, near the Paquier.
ο	Al 3-4	*Mi.rischi*	NC 8A-B	Abrupt break on $\delta^{13}C$ increasing trend in the *Mi. rischi/planispira* foraminiferal zone, Urbino event.

and high amplitude oscillation, marking the Kilian sub-event in the Tethyan realm (Bréhéret, 1983, 1988). The next interval is characterized by a decreasing trend representing Ap12-14, of which the lowest values are associated with the onset of OAE 1b event. Within the following decreasing trend, a rapid fluctuation occurs in the correspondence of the Kilian Level, a standout feature near the Aptian-Albian boundary (Bornemann et al., 2023; Coccioni et al., 2014; Herrle et al., 2004, 2015; Leandro et al., 2022). The Kilian Level, labeled here as **λ** marker, is one of the most prominent features at the Aptian-Albian interval and an important marker for approximating the Aptian-Albian boundary (Charbonnier et al., 2023; Coccioni et al., 2014; Petrizzo et al., 2012). It is characterized by a $\delta^{13}C$ positive excursion followed by a negative excursion in the Tethyan realm (Vocontian Basin and UMB).

The **μ** marker is a positive $\delta^{13}C$ shift in the *Mi. renilaevis* foraminiferal zone, above the Kilian negative peak. This level is associated with an age of 113 Ma (Gale et al., 2020). The Vöhrum's tuff was identified above the Killian's excursion (Bornemann et al., 2023). The Kilian Level (top of Ap 15 C-stratigraphy stage or FO of *M. renilaevis*) shows a very minor positive excursion in the Atlantic Ocean (Axel Heiberg Island, North Atlantic Ocean) (Figure 4a). The Cedar Mountain Formation (USA) $\delta^{13}C$ curve also reveals a similar pattern (Ludvigson et al., 2010).

Herrle et al. (2015) positioned the Kilian Level quite distant from the Albian base, with a U-Pb absolute age of 111.74 ± 0.26 Ma, using bentonite zircons for an interval remarkably close to the Kilian Level (~550 m; Figure 4a). In our correlation, this age corresponds to an interval close to **ξ** marker. Therefore, the signature that Herrle et al. (2015) attributed to the Kilian Level, is here correlated to the Paquier (**ξ** marker) or Urbino Level (Charbonnier et al., 2023; Coccioni et al., 2014). Consequently, the interval attributed to the OAE 1b at Axel Heiberg Island (Herrle et al., 2015) is here related to the Leenhardt Level (Charbonnier et al., 2023; Coccioni et al., 2014), and represented as a **ο** marker.

The **ξ** marker represents a negative peak associated with the Paquier Level in the Vocontian Basin (Herrle et al., 2004), and a ~0.4‰ fluctuation corresponding to the Urbino Level in the PLG record (Coccioni et al., 2014). Above, in the Al3-5 interval, the $\delta^{13}C$ curve reaches a minimum and then increases. Below the **ν** marker,

oscillations occur within the Monte Nerone interval at PLG without significant expressions in the isotopic curve in the Vocontian Basin, despite correlations between Monte Nerone and Levels HN 3-HN 7 (Coccioni et al., 2014; Herrle et al., 2004). The Invincible Point Member of the Christopher Formation was dated at 111.74 Ma using bentonite zircons and falls close the **o** marker in the Axel Heilberg Island (AHI) section (Herrle et al., 2015). The exact stratigraphic positioning of this dating is difficult to correlate with PLG and Vocontian sections, and thus, this was used solely as an age control point for the upper boundary of the studied section in the tuning process.

3.5. Cyclostratigraphy

As discussed previously, our studied interval partially overlaps the upper record of the PLG core investigated by Leandro et al. (2022), in order to verify whether the 405-kyr-based ATS inferred by these authors could be extended upwards, hence reaching the OAE 1b interval. The sedimentation rates based on previous studies of astrochronology and biostratigraphy of the PLG (section and core) are spanning around ~0.5 cm/kyr (Coccioni et al., 2014; Leandro et al., 2022). Considering the sampling resolutions of the XRF-derived series (Fe and Ti data–carried out every 5 cm) and of the MS series (every 2.8 cm), the overall performed resample of all proxies to 2 cm within the cyclostratigraphic analyses did not impact the recognition of the Milankovitch cycles.

The MTM-based spectral analysis for the MS data (Figure 5) evidenced a spectral content which is pervasive throughout the PLG core stratigraphy and exceeded both the 95% CL and the 95% F-test significance level, with a spectral peak ratio of 214:66:56:22:12 = 17.8:5.5:4.7:1.8:1. A similar pattern is also identified for the Fe and Ti data sets (Figure 6), with a set of statistically significant spectral peak content (Ti data–204:66:55:21:11 = 18.5:5.9:5.0:1.9:1) and (Fe data–219:65:55:23:11 = 19.9:5.9:5.0:2.1:1). The three spectral peak ratios resemble the predicted Milankovitch spectral peak ratios for Albian times (405:125:95:39.7:22.9 = 17.7:5.5:4.2:1.7:1; Waltham, 2015).

In combination with the eFFT analysis, it was possible to suggest that the 0.21–0.86 cycles/m (496–115 cm) and 1.06–2.00 cycles/m (94–50 cm) frequency bands observed for the MS data set (Figure 5c) would be related to the expression of the g_2–g_5 (long) and g_4–g_2 and g_4–g_5 (short) eccentricity cycles, respectively. Similarly, the same features were also observed for the Ti (long eccentricity band: 0.25–0.97 cycles/m (389 and 102 cm)/short eccentricity band: 1.09–1.87 cycles/m (91 and 53 cm)) and Fe (long eccentricity band: 0.24–1.04 cycles/m (407 and 95 cm)/short eccentricity band: 1.09–2.26 cycles/m (91 and 45 cm)) data sets (Figures 6b and 6e, respectively). Such interpretation is in accordance with Leandro et al. (2022), as two long eccentricity cycles would be expected between the Jacob and Kilian Levels (comprising a ~810 kyr timespan) and hence the 405-kyr cycle should have an approximate wavelength of ~214 cm (~0.47 cycles/m). Frequency bands of 2.28–2.61 cycles/m (43 and 38 cm) (MS data; Figure 5c), 1.95–3.28 cycles/m (51 and 30 m) (Ti data; Figure 6b) and 2.43–3.45 cycles/m (41 and 29 cm) (Fe data; Figure 6e) were interpreted as a ~80 kyr transient imprint, which has been reported for Phanerozoic records worldwide (e.g., Leandro et al., 2022; Wu et al., 2013). Furthermore, it was possible to suggest the imprint of the obliquity (MS (Figure 5c): 3.24–5.90 cycles/m (30–17 cm)—Ti (Figure 6b): 3.76–7.06 cycles/m (26–14 m)—Fe (Figure 6e): 3.59–6.98 cycles/m (27–14 cm)) and precession (MS (Figure 5c): 6.28–12.67 cycles/m (16–8 cm)—Ti (Figure 6b): 7.20–12.20 cycles/m (13–8 cm)—Fe (Figure 6e): 7.06–12.19 cycles/m (13–8 cm)) spectral bands.

As previously discussed, the ASM method (Meyers & Sageman, 2007) was applied aiming to provide a clear statistical test for rejecting the null hypothesis, by detecting statistically significant harmonic components and estimating the uncertainties associated with the astronomical signals in the MS stratigraphic data series (Figures 5e–5g; Table 2). By considering the vectors of "candidate" (0.47, 1.51, 1.77, 2.19, 2.39, 4.60, 8.09 cycles/m) and theoretical astronomical frequencies, as well as the Nyquist frequency (=25 cycles/m) carried out from the MS data, we found an optimal sedimentation rate of ~0.525 cm/kyr (ASM = 1.53×10^{-4} cycles/kyr) characterized by the lowest H_0-significance level (0.001%). It surpassed the critical significance level and hence led us to reject the null hypothesis for random signal with a high degree of confidence. Furthermore, it is compatible with the orbital interpretation of Leandro et al. (2022) and supports the sedimentation rates based on biostratigraphy (Coccioni et al., 2014).

The eCOCO analysis of the MS data set reveals a mean sedimentation rate of 0.56 cm/kyr, with a significance level $<10^{-3}$ (Figures 7b and 7c). Although other spectral peaks (~1.8 and 2.4 cm/kyr) are present in the eCOCO map, they do not exceed the considered null hypothesis threshold (Figure 7c). The COCO/eCOCO analysis of the MS data set reveals a mean sedimentation rate of 0.56 cm/kyr, with a significance level $<10^{-3}$ (Figures 7b and 7c). Although other spectral peaks (~1.8 and 2.4 cm/kyr) are present in the eCOCO map, they do not exceed the

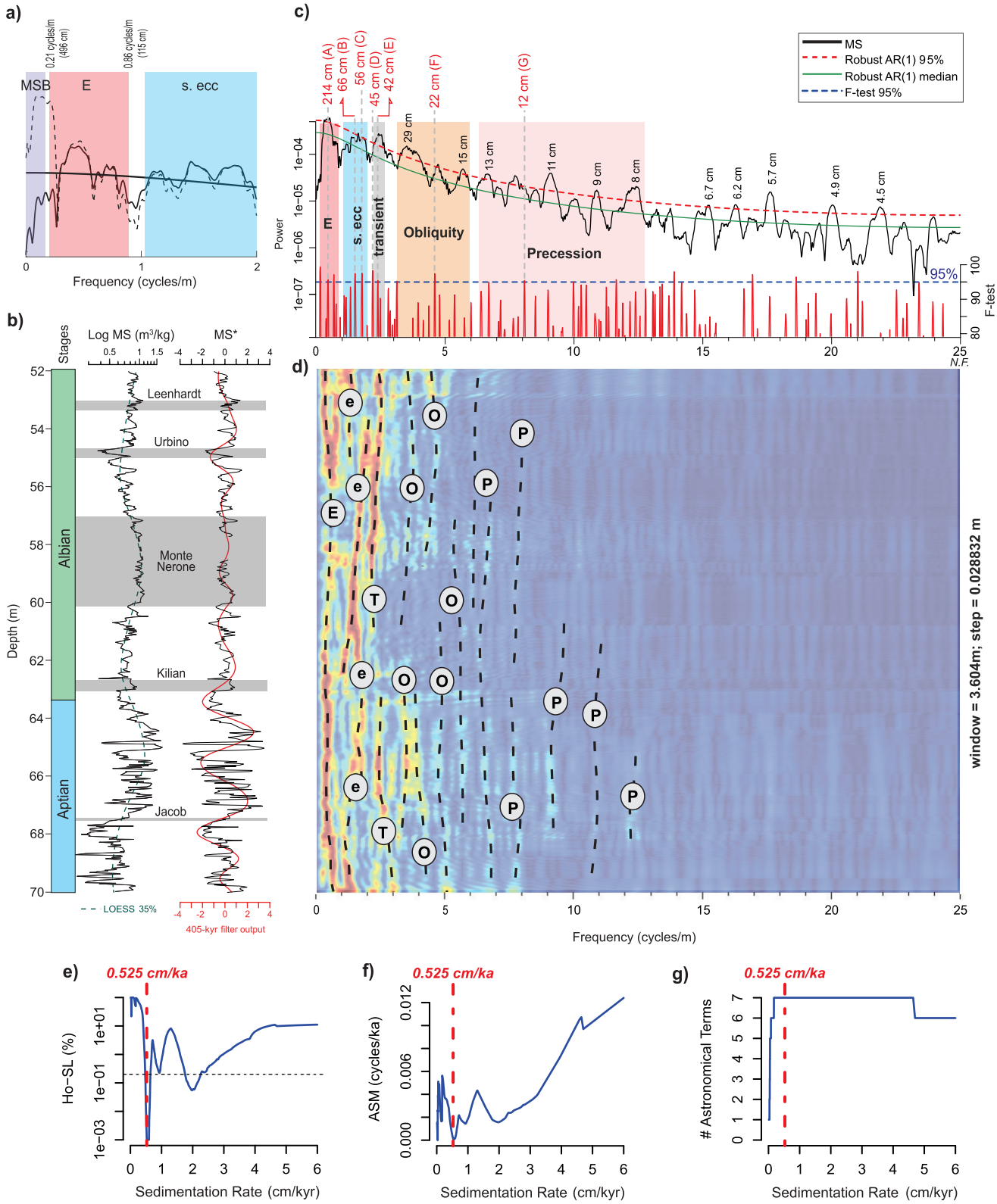

Figure 5.

null hypothesis threshold considered (Figure 7c). The number of orbital parameters in the COCO analysis, as well as its evolutionary version, indicates optimal rates of up to ~2 cm/kyr (Figure 7d). Through the combination of eCOCO and the evolutionary null hypothesis level (eCOCO*H_0SL) (Figure 7e), it is possible to infer that the sedimentation rate throughout most of the PLG core likely varied between 0.4 and 0.6 cm/kyr, which appears consistent with previous astrochronology and biostratigraphy-based studies on the PLG (~0.5 cm/kyr; Coccioni et al., 2014; Leandro et al., 2022).

3.5.1. Phase Relationship of MS Data and La04 Astronomical Solutions

Prior to the astronomical tuning, we evaluated the signal phase of the 405-kyr sinusoidal curve carried out from the MS data set in order to verify whether transfer functions linked to the paleoclimate and environmental non-linear responses may altered the amplitude and phase of the signal regarding the astronomical solution. We applied the TimeOpt method (Meyers, 2015) (Figure 8), which allowed us to estimate the amplitudes and phases of astronomical periods during model optimization, and if it also reflects non-linear responses from the Earth system (Meyers, 2019). The evolutionary TimeOpt analysis (eTimeOpt; Figure 8b) indicated sedimentation rates values between 0.40 and 0.75 cm/kyr throughout the PLG interval with a confidence level greater than 95%. In order to ensure a more accurate evaluation, we focused on the interval between 55 and 63 m (black-dashed rectangle; Figure 3b).

We considered for TimeOpt evaluations the following information: (a) sedimentation rate values ranging from 0.1 to 0.8 cm/kyr, based on prior average background estimates (e.g., Coccioni et al., 2014; Leandro et al., 2022); (b) mean age of ~113 Ma (=Kilian Level mean age according to GTS2020); (c) along with precession modulation and Taner bandpass cut-off frequencies (Taner, 1992) of 0.035 and 0.065 cycles/kyr; (d) precession and eccentricity targets derived from the La04 solutions (Laskar et al., 2004); and (e) 2000 Monte Carlo simulations (AR1). We carried out an optimal sedimentation rate of 0.47 cm/kyr by means of the time-calibrated envelope fitting to the TimeOpt-reconstructed model (Figure 8d). The spectral power regression model identifies maximum r^2_{opt} of 0.044 (Figure 8e). A Monte Carlo-based independent analysis of 0.47 cm/kyr SAR peak resulted in: $r^2_{envelope} = 0.366$; $r^2_{power} = 0.159$; $r^2_{opt} = 0.044$ (Figure 8g). Despite the good correlation given by $r^2_{envelope}$, some misalignments can be noticed. It could be possibly explained by amplitude losses at the precession envelope at the study interval due to spatial drift, which distorts the astronomical cycles and placing the precession cycles outside the bandpass region (Meyers, 2019).

Particularly, the Vöhrum tuff is stratigraphically positioned above the carbon isotope negative excursion of the Kilian Level in the Dolgen 3 core (Bornemann et al., 2023), approximately 20 m above the most negative peak of the $\delta^{13}C$ excursion and the First Appearance Datum of *Prediscosphaera columnata* (*P. columnata*) in the Dolgen 3 core, as shown in Figures 4 and 9. This carbon isotope negative excursion allows us to correlate the Dolgen 3 core with the PLG core at a depth less than 62.6 m (top of the Kilian Level). As previously demonstrated, the "cave-cave" correlation between the 405-kyr component in the MS* and the La2004 (La04) astronomical solution remains valid. Filtering the 405-kyr component of the MS* signal positions the top of the Kilian Level near (within 50 cm of) a peak in maximum eccentricity within a 405-kyr cycle, indicating that the Vöhrum tuff is close to the maximum eccentricity, regardless of the filter used to isolate the 405-kyr component from the MS. It is also corroborated by assessing potential phase variations on the frequency band between distinctive filtering methods (Dynamic, Lowpass, Taner, or Gauss, Figure 9a). Noteworthy, the stratigraphic differences between the maximum values of these filters are at most 20 cm. Assuming a rate of ~0.5 cm/kyr, such discrepancies are equivalent to ~0.4 kyr depending on the filter used (Figure 9a). In this study, we chose to use dynamic filtering because it provides better control in isolating the 405-kyr sinusoidal component, as discussed in Section 3.5.2.

Figure 5. (a) Low frequency spectral range exhibiting the raw (dashed line) and 35% "loess" detrended MS data, indicating the preservation of eccentricity frequency bands (E: long eccentricity band, in pale red; s. ecc: short eccentricity band, in blue). MSB: million-year scale band. (b) Representation of Oceanic Anoxic Event 1b sub-events (gray bands) associated with the Aptian-Albian section of the Poggio le Guaine core. Left: MS (black) and 35% "loess" detrending (green) curves; Right: MS* (MS data after 35% "loess" detrending, black line) associated with the 405-kyr filtering output (red line). (c) Top: MTM power spectra with the AR(1) red noise spectra model and 95% confidence level (CL). Bottom: F-test results (red line) highlighting the 95% CL (dashed blue line). The dashed gray lines represent the orbital cycles described in Table 1 (highlighted in red). (d) Evolutionary harmonic analysis (EHA). The dashed line indicates the traces of candidate orbitally-induced signals. (e) H_0-significance level for the Average Spectral Misfit (ASM) test (given a sedimentation rate ranging from 0.01 to 6.0 cm/ka, 500 sedimentation rates investigated in ASM optimization grid, and a number of Monte Carlo simulations equal to 100,000). The dashed line indicates the critical significance level. (f) ASM results indicating ~0.525 cm/kyr as an optimal sedimentation rate. (g) The number of astronomical terms available for calculation of ASM.

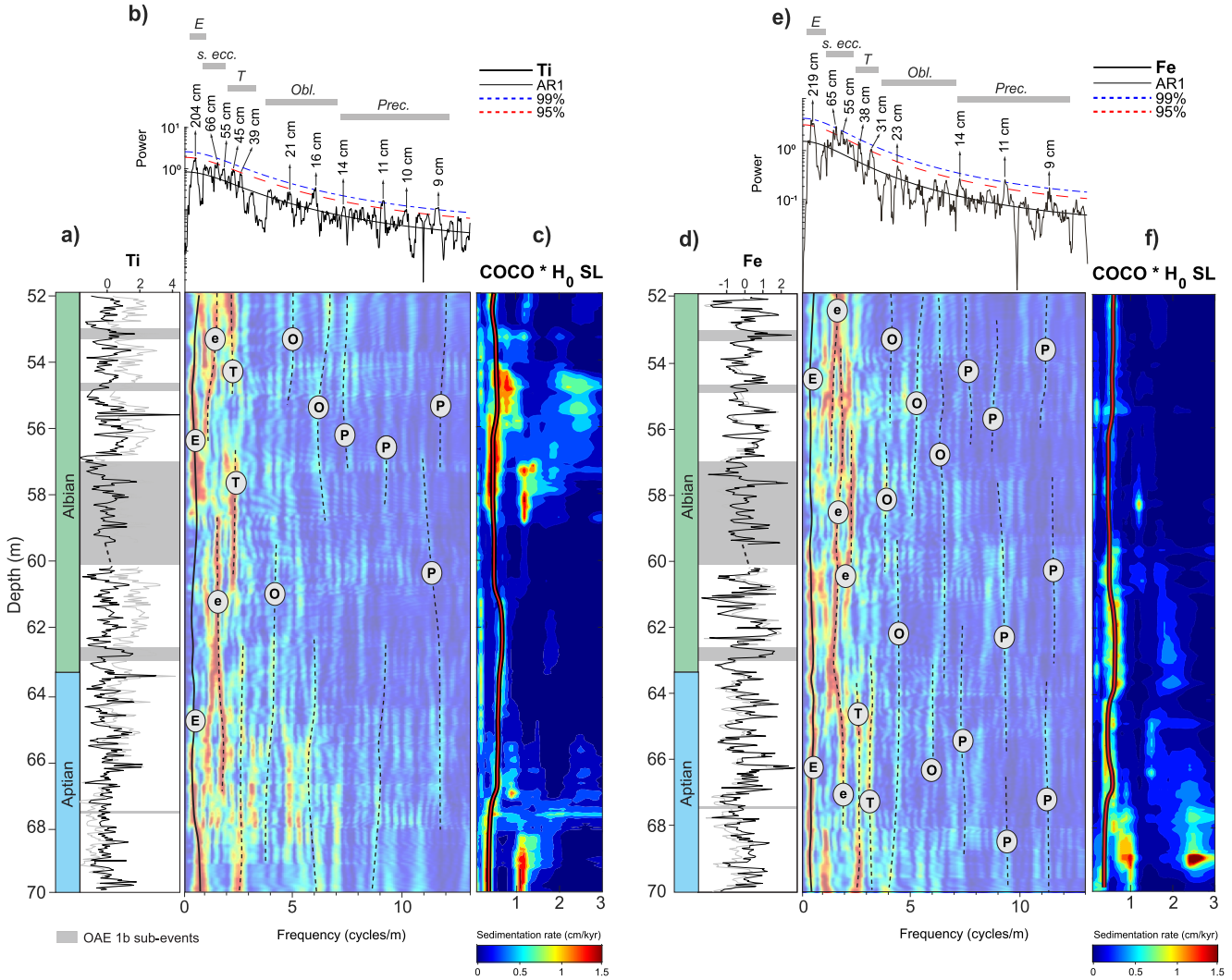

Figure 6. Cyclostratigraphic analyses for the Ti and Fe depth-domain data sets for Poggio le Guaine (PLG) core (after 35% "loess" detrending). (a) Representation of Oceanic Anoxic Event (OAE) 1b sub-events (gray bands) recorded at the Aptian-Albian section of the PLG core, associated to the Ti data (black line). (b) Top: MTM power spectra for the Ti data set associated with the AR(1) red noise spectra model and 95% and 99% confidence levels (CLs). Bottom: Evolutionary harmonic analysis for the Ti data set. The dashed line indicates the traces of candidate orbitally-induced signals. (c) Combinate map of ρ and H_0SL (COCO* H_0SL) used to track sedimentation rates (red line) at the Ti data. (d) Representation of OAE 1b sub-events (gray bands) recorded at the Aptian-Albian section of PLG core, associated with the Fe data (black line). (e) Top: MTM power spectra for the Fe data set associated with the AR(1) red noise spectra model and 95% and 99% confidence levels (CLs). Bottom: Evolutionary harmonic analysis for the Fe data set. The dashed line indicates the traces of candidate orbitally-induced signals. (f) Combinate map of ρ and H_0SL (COCO* H_0SL) used to track sedimentation rates (red line) at the Fe data.

3.5.2. Astronomical Tuning

In this study, we opted to use dynamic filtering as it allows better control in isolating the 405-kyr sinusoidal component. It was conducted by tracking the highest power of the 405-kyr signal throughout the PLG core. At the uppermost portion of the core (~52–54 m), the tracked frequency ranged from 0.21 to 0.47 cycles/m. From a depth of ~54 m, the signal exhibited higher frequencies, ranging from 0.27 to 0.80 cycles/m. Between ~55.9 and 57.9 m, the 405-kyr signal is not preserved in the eFFT analysis; thus, the same frequencies (0.27–0.80 cycles/m) were applied for filtering within this interval. From a depth of 58.1 m, the signal reappears in the eFFT analysis, with frequencies ranging from 0.35 to 0.86 cycles/m, and after 59.6 m, the frequencies gradually decrease (~0.24 to ~0.61 cycles/m) down to a depth of 67.7 m. From 67.7 m to the base of the PLG core, the frequencies used for filtering ranged from 0.25 to 0.79 cycles/m.

Table 2
Summary of the Average Spectral Misfit Results

ID	Frequency (cycles/m)	MTM probability (%)	M-cycles	Period (kyr)
A	0.47	95.6	E1	405
B	1.51	97.5	E2	131/125
C	1.77	97.6	E3	99/95
D	2.19	98.4	T1	
E	2.39	95.5	T2	
F	4.60	97.5	O1	p + s3
G	8.09	95.4	P1	p + s1/p + s2
	# orbital parameters:	7		
	ASM:	0.000153		
	***p*-value:**	1.00E−05		
	Null Hypothesis (%):	0.001		

If we anchor the Kilian Level to cycle A (with maximum eccentricity at 113.55 Ma), the peak eccentricity associated with the tuff would fall outside the plausible age range (being older). Similarly, fixing the Kilian Level at the inflection point of cycle C (112.74 Ma) would also place the maximum eccentricity beyond the acceptable age range. By analyzing the relative positions of the inflection points and the hypothetical stratigraphic position of the tuff, we conclude that cycle B is the best candidate for anchoring the top of the Kilian Level at ∼113.14 Ma.

Laskar's astronomical solutions, widely used in stratigraphic astrochronology, account for the chaotic motion of the solar system (Laskar, 1989, 1990). The g_2–g_5 term (405-kyr metronome) is utilized for time calibration of the stratigraphic record (Laskar, 2020). The phase lag between the classical La04 solution and more recent solutions (La10a, La10b, La10c, La10d; Laskar, Fienga, et al., 2011, Laskar et al., 2004) introduces an error of 120 kyr (phase lag between La04 and La10b) into the ages recovered through astronomical tuning (Figure 9d). Our 405-kyr tuned age model for the PLG core is based on the g_2–g_5 target curve from the La04 solution.

The astronomically tuned MS curve (Figure 10) was constructed by aligning the ∼200 cm component of the MS series with the 405-kyr term of the La04 solution (Laskar et al., 2004). Using a dynamic filter with cut-off frequencies between 0.21 and 0.86 cycles/m, we isolated the 405-kyr long-eccentricity component within the MS data set (Figure 10a). Orbital tuning was performed with 9 tie points over a ∼3.6 Myr interval using the Acycle software (Li et al., 2019). Based on phase analysis (Meyers, 2019), we aligned the 405-kyr component of the MS maxima with maxima in the La04 eccentricity 405-kyr component. We also aligned the minimum values to refine the sedimentation rates.

The exact stratigraphic distance between the peak maximum of eccentricity in the 405-kyr component and the Vöhrum tuff correlate in the PLG core is not precisely known. The tuning process associates the peak maxima of eccentricity from the filtered 405-kyr MS series (input) with the La04 solution (target). Therefore, the maximum potential error during tuning is 405 kyr (the duration of one cycle). Given the proximity between the top of the Kilian Level and the Vöhrum tuff, we use the maximum temporal deviations of ∼120 kyr from other Laskar orbital solutions to estimate errors in our astronomically calibrated ages for biostratigraphic events, organic-rich levels, and carbon isotope markers (c-markers, Section 3.4). For each event, the estimated age error was considered as the full temporal deviation (in kyr) between La04 (Laskar et al., 2004) and La10b (Laskar, Fienga, et al., 2011, Laskar et al., 2004) eccentricity peaks (Figures 9d and 10).

Figure 10a shows the Loess detrended Log MS data set and the 405-kyr dynamically filtered signal used for tuning, anchored with red (111.74 ± 0.26 Ma, Herrle et al., 2015) and blue arrows (113.1 ± 0.3 Ma, Selby et al., 2009), and the stratigraphic position of CIS (Greek letters, in red). The alignment of maximum and minimum eccentricities allowed us to construct a FATS based on 9 long-eccentricity cycles (E_3 to E_{-5}, marked in red, where E_0 corresponds to the Kilian Level, Figure 10c) and to develop an age model for the studied interval (52–70 m) in the PLG core, spanning ∼3.6 Myr (Figure 10d). The tuning process and eCOCO analysis (Li et al., 2019) revealed an mean sedimentation rate of ∼0.5 cm/kyr for the PLG core interval (Figure 10b). The

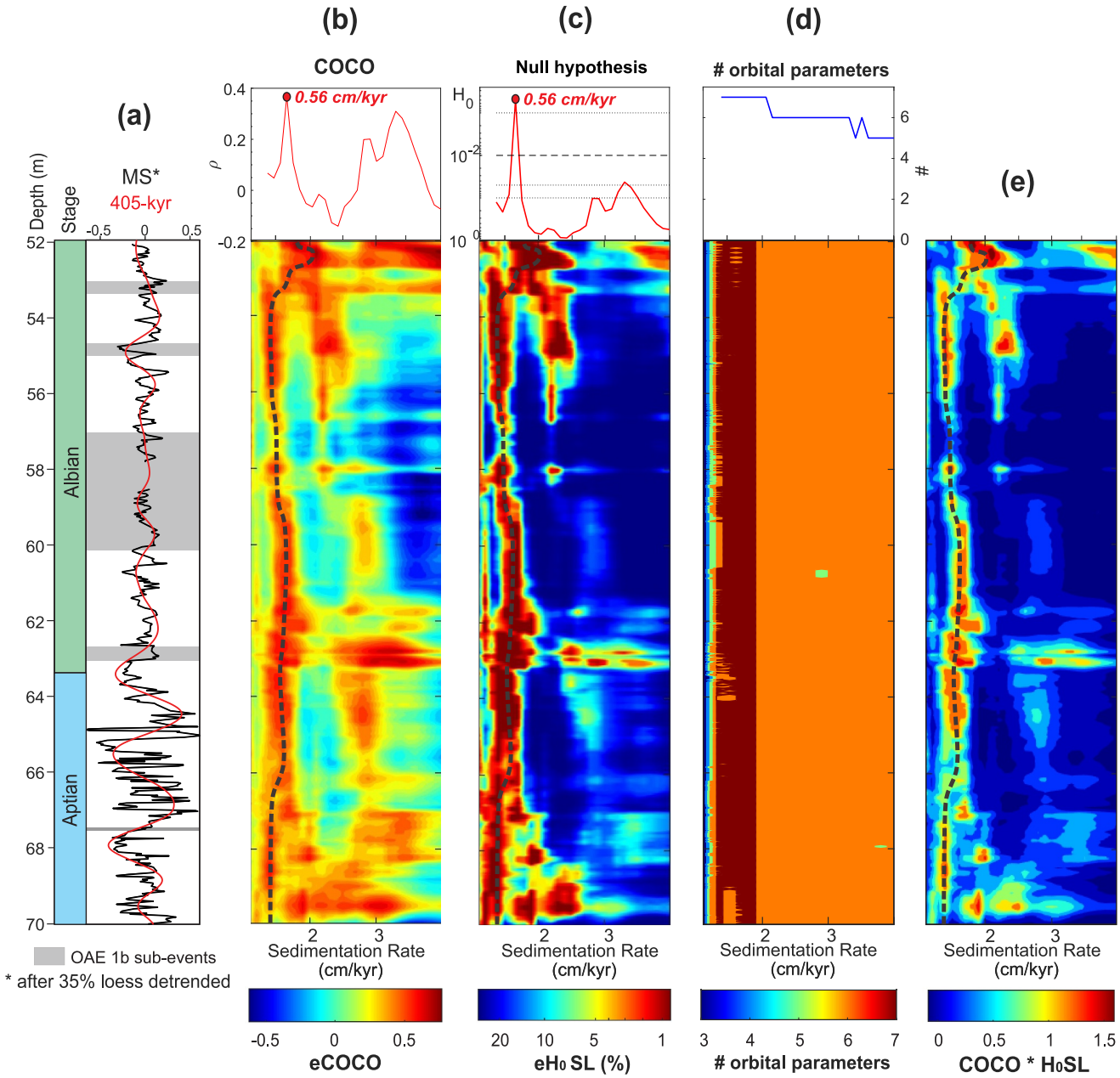

Figure 7. COCO/eCOCO analysis of the Poggio le Guaine core MS data series. (a). MS data (after 35% "loess" detrending associated with the 405-kyr sinusoidal filtering curve (black and red lines, respectively). (b) COCO and evolutionary ρ map (eCOCO). (c) Null hypothesis (H_0, no astronomical forcing) and evolutionary H_0 significance level (eH_0SL) map. (d) Number of contributing astronomical parameters and evolutionary map of the number of contributing astronomical parameters. (e) Combinate map of ρ and H_0SL used to track sedimentation rates (SRs) along the interval. f) Evolutionary r^2_{opt} map together with tracked highest eCOCO*SL*#orbits values. Evolutionary COCO analysis employed 2000 Monte Carlo simulations, sedimentation rates ranging from 0.1 to 3.0 cm/kyr (step of 0.1 cm/kyr), La04 (Laskar et al., 2004) solution with a mean age of ~113 Ma as reference (maximum frequency of 0.06 kyr^{-1}).

sedimentation rate increases from 0.42 to 0.65 cm/kyr until reaching the Monte Nerone Level, then decreases to 0.47 cm/kyr, indicating a paleoenvironmental shift marked by a noticeable change in sediment coloration from greenish to reddish.

The orbital tuning allowed us to build a FATS for the OAE 1b interval (from the base of the Jacob Level to the top of the Leenhardt Level), covering a timespan of ~2.84 Myr. Based on the MS data age model, we inferred ages of ~113.56 ± 0.12 Ma and ~113.36 ± 0.12 Ma for the First Occurrence (FO) and Last Occurrence (LO) of *M. miniglobularis* ~113.36 ± 0.12 Ma and ~112.80 ± 0.12 Ma for FO and LO of *M. renilaevis*, with the latter

10.1029/2024PA004860

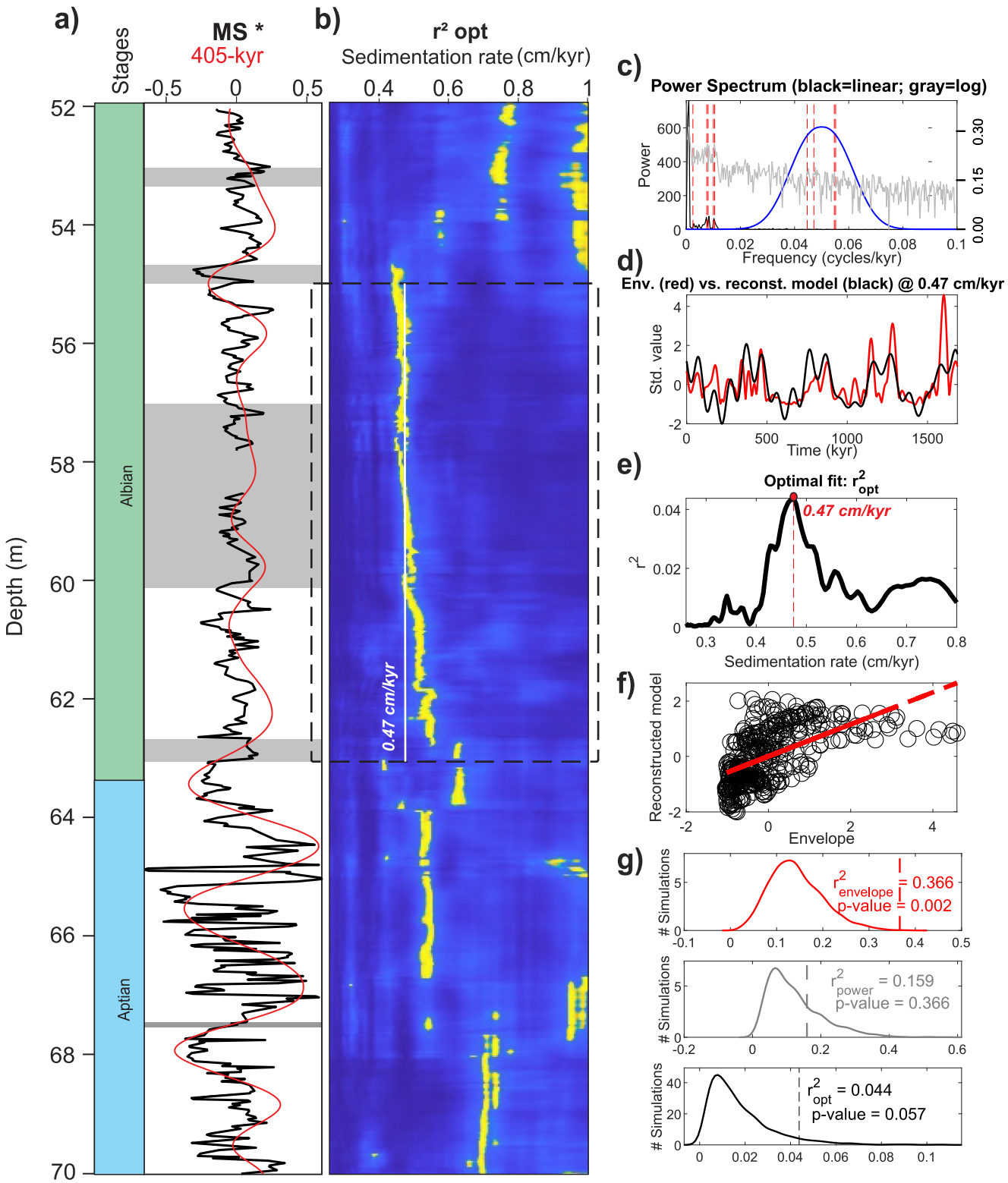

Figure 8.

coinciding with the FO of *Microhedbergella rischi (M. rischi)*. We also estimated ages for major black shale levels in the PLG core.

Carbon isotope curve correlations (Figure 4) allowed us to infer a second tie point. By using the carbon curve from Axel Heiberg (Herrle et al., 2015), we employed the age of 111.74 ± 0.26 Ma (approximately the **o** marker) as a control age for the upper portion of the studied interval. Although this dating is of excellent quality, the carbon isotope curve correlation between Axel Heiberg and PLG is less clear than the correlation using the negative excursion of the Kilian Level. Consequently, we used it solely as a temporal control point. After the tuning process, we determined an age of 111.52 ± 0.12 Ma for the extrapolated stratigraphic position of this dating in the PLG, further strengthening the robustness and reliability of our astrochronological interpretation.

4. Discussion

4.1. Upper Aptian/Lower Albian FATS in the PLG Core and C-Isotope Correlations

Our work provided a detailed upper Aptian-lower Albian time-depth framework for the PLG core. Through an astronomically calibrated age model, we were able to obtain the ages of OAE 1b sub-events and various zonal markers of calcareous nannofossils, correlating them with planktonic foraminiferal zonal markers (Coccioni et al., 2012, 2014; Leandro et al., 2022; Sabatino et al., 2015, 2018). Previous studies have used a different age assumption, which was based on duration of Albian Stage (Grippo et al., 2004; Huang et al., 2010). Leandro et al. (2022) used new M0r ages (Zhang et al., 2021) associated with high-precision U-Pb date of 113.1 ± 0.3 Ma (Selby et al., 2009) and provided a new age model for the Aptian Stage based on 405-kyr astronomical tuning with the g_2–g_5 target curve from the La2004 solution for the Aptian–Albian.

Using SAR techniques (COCO/eCOCO, ASM and TimeOpt; Li et al., 2018; Meyers, 2015, 2019) we were able to estimate a sedimentation rate ranging from 0.4 to 0.6 cm/kyr for the studied interval. SAR slightly increases following the same trends of Ti and Fe contents, until the onset of the Monte Nerone black-shales cluster, where it drops below 0.5 cm/kyr and then it remains steady up to the Urbino Level. This result is consistent with the eTimeOpt/COCO/eCOCO results (Figures 7, 8 and 10).

As the MS data set partially overlaps with the upper record of the PLG core studied by Leandro et al. (2022), we obtain similar SAR (mean of 0.6 cm/kyr) in the same intervals. The main difference lies in the tiepoint used to anchor the 405 kyr long-eccentricity cycles. Vöhrum's tuff layer above carbon isotope negative excursion associated to the Kilian Level at Dolgen 3 core (Bornemann et al., 2023) allows us to anchor the 405-kyr component at 113.24 Ma (by using the solution La2004, Figure 9), hence providing greater precision to the tuning process since there is no longer a need to use the average value of 113.00 Ma as an anchor. Table 3 shows estimated age for major OAE 1b sub-events.

Previous studies have suggested a correlation between OAE 1a with the OJP basalt flows (Chambers et al., 2004; Larson & Erba, 1999; Tejada et al., 2009) and a rapid global warming, and elevated rates of silicate weathering on the continents (Bottini & Erba, 2018). However, new age constrains of the OJP show that the upper lava-flow units are much younger (i.e., 115.51–111.42 Ma) than previously suggested (Davidson et al., 2023). These numbers are consistent with our study, where the effect of enhanced weathering began near the onset of the 113/Jacob Level, marked by increasing sedimentation rate and Ti and Fe contents into the UMB. $^{187}Os/^{188}Os$ pulses related to the OAE 1b (Matsumoto et al., 2020) also support this suggestion (Figure 2). The apparent diachronism between the onset of anoxic events in different sections (e.g., Kilian at 112.9 Ma in Leandro et al., 2022 and 113.6 Ma in Fauth et al., 2022) from different global regions may be attributed to age adjustments (anchor *bias*) and $\delta^{13}C$ correlation errors, as it can be observed in Figure 9.

Figure 8. Evaluation of the signal phase of MS* (MS after 35% "loess" detrending) data set and sedimentation rates using TimeOpt and eTimeOpt analysis. Black, dash line rectangle represents the stratigraphic interval which was considered for the TimeOpt evaluations. (a) MS* data of Poggio le Guaine core; (b) Evolutionary r^2_{opt}. The yellow colors represent confidence levels above 95%; (c) Fit of the target periods to the observed periods using the sedimentation rate of 0.47 cm/kyr; (d) Comparison between the data amplitude envelope (red) and the TimeOpt-reconstructed model (black); (e) Combined envelope and spectral power fit (r^2_{opt}) at each evaluated sedimentation rate; (f) Cross plot of the data amplitude envelope and the TimeOpt-reconstructed model; (g) Monte Carlo simulations of different sedimentations rate of the bulk TimeOpt analysis.

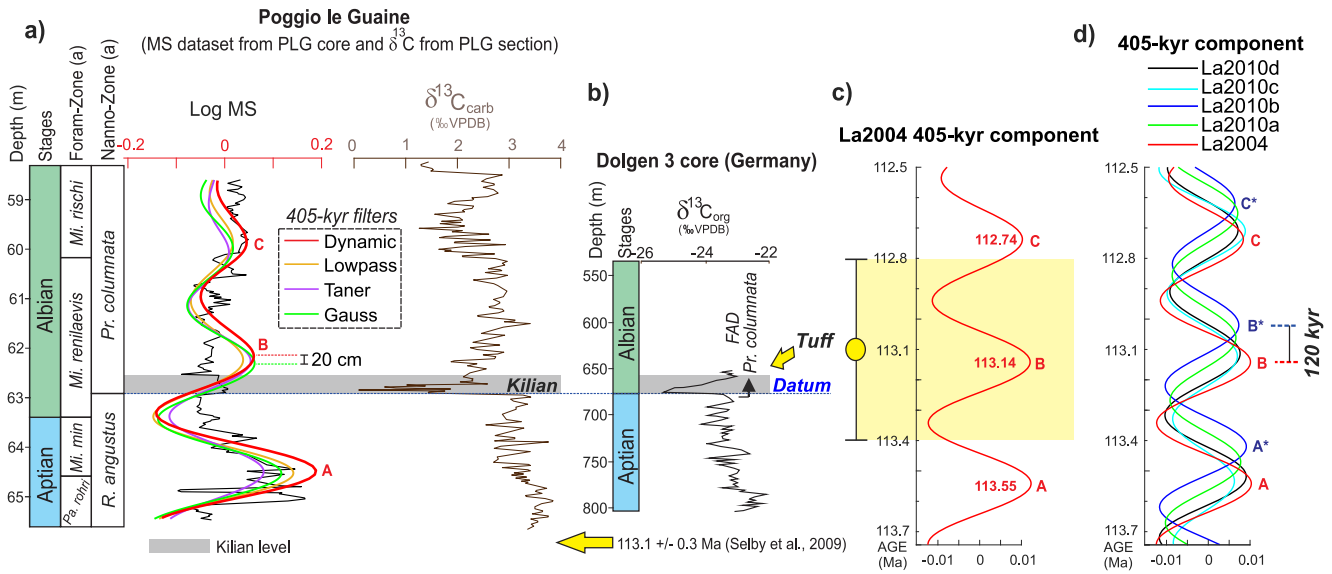

Figure 9. Evaluation of the signal phase of MS*-based 405-kyr sinusoidal curve (MS after 35% "loess" detrending) at the Kilian Level based at La04 solution (Laskar et al., 2004). (a) The Kilian Level at Poggio le Guaine together with biozones (Coccioni et al., 2014) and 405-kyr sinusoidal curve; (b) Vöhrum's tuff stratigraphic position at Dolgen 3 core (Bornemann et al., 2023); (c) Overlap of the error range in Vöhrum's tuff absolute dating (Selby et al., 2009) with the La04 solution 405-kyr component; (d) Comparison of phases of 405-kyr long eccentricity of La04, La10a, La10b, La10c, La10d solutions (Laskar et al., 2004, 2011a, 2011b). Yellow arrow indicates Vöhrum's tuff stratigraphic position at Dolgen 3 core.

After comparing the ages of OAE 1b sub-events, we must double-check their stratigraphic position with respect to the our C-isotope markers (Figure 4). The 113/Jacob Level of Huang et al. (2010) occurs near the base of the *Nannoconus regularis* calcareous nannoplankton zone and within the *P. rohri* planktonic foraminiferal zone. Nonetheless, it is important to mention that these two works used different tiepoints: Huang et al. (2010) used the Albian-Cenomanian boundary at 99.6 Ma as a tiepoint for the tuning process, without using any absolute radiometric age to anchor this boundary, while Charbonnier et al. (2023) employed the average age of the base of the Albian (113.2 ± 0.3 Ma by Gradstein et al. (2020), after U-Pb dating of Selby et al. (2009)) in the tuning process.

The high latitude Kilian Level of Herrle et al. (2015) corresponds to the benthic *Verneuilinoides borealis* foraminiferal zone and has a carbon isotope pattern that is quite distinct from other patterns for the Kilian Level (Bodin et al., 2023; Charbonnier et al., 2023; Coccioni et al., 2014; Huang et al., 2010; Kennedy et al., 2014, 2017; Leandro et al., 2022), represented here by the **λ** marker. In general, the Kilian Level is visible in C-isotope curves as a positive excursion followed by a negative excursion, associated with *M. renilaevis* foraminiferal zone (Kennedy et al., 2014, 2017). The Vöhrum section and the ash layer at 113.1 ± 0.3 Ma (Selby et al., 2009) do not contain planktonic foraminifera, and the correlation between the two outcrops is based on ammonite associations (top of *Hypacanthoplites jacobi* ammonite zone) and the FO of *P. columnata* (subcircular category). *H. jacobi* ammonite zone extends into the early Albian standard zonation of Ogg et al. (2016) and could be correlated not only with the Kilian Level (Bodin et al., 2023) but also with HK 3–6 key beds (Monte Nerone, in PLG) and the Paquier Level (Herrle et al., 2010). Thus, the Aptian-Albian boundary in the Vöhrum section (Selby et al., 2009), does not necessarily coincide with the Kilian Level and the age of 113.1 ± 0.3 Ma could be the age of the Ap-15, Al-1 or Al-2 CIS (Herrle et al., 2010).

Our astronomical tuning provides an age of 112.80 ± 0.12 Ma for the base of the Monte Nerone interval (Coccioni et al., 2014) and of 111.70 ± 0.12 Ma for the Urbino black shale Level (**o** marker), remarkably close to the U-Pb 111.74 ± 0.26 Ma of the dated and extrapolated level of Herrle et al. (2015). For the **μ** marker, the Vöhrum tuff, we estimate an age of 113.20 ± 0.12 Ma, which corroborates the 113.1 ± 0.3 Ma of the ash layer (Bornemann et al., 2023; Selby et al., 2009).

Cyclostratigraphic analysis of Nebe (1999) estimated a median age of 113.25 Ma for the Kilian Level. The present work provides an age of 113.28 ± 0.12 Ma for the **λ** mark (extreme point of negative excursion associated to the Kilian Level, PLG core) and 113.32 ± 0.12 Ma for the **κ** mark (extreme point of positive excursion),

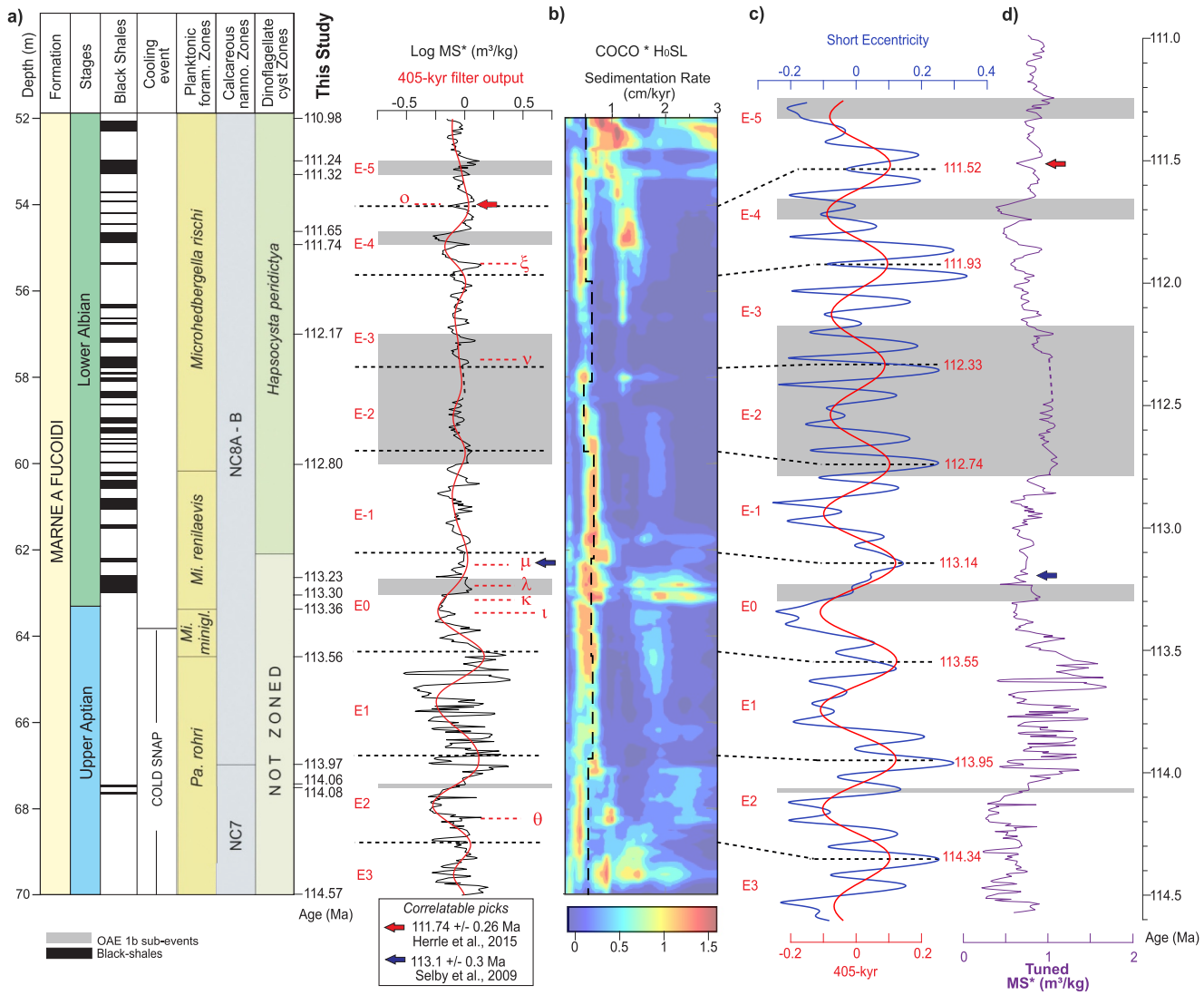

Figure 10. Astronomical calibration of the Poggio le Guaine core: (a) MS* (MS after 35% "loess" detrending) data and 405-kyr component filtered using dynamic filter, and (E) cycles denoted in red. The E-cycles and C-marks are presented in red letters and red and blue arrows represent transposed absolute ages used as tiepoints. Calcareous nannofossil, planktonic foraminiferal biostratigraphy and black shales from Coccioni et al., 2012, 2014, updated with astrochronological ages. Cold Snap (McAnena et al., 2013) boundary from Leandro et al. (2022). (b) The SAR curve recovered on 405-kyr tuning process (dashed black) and COCO*H_0SL. (d) La04 solution for the eccentricity cycles of ~100 kyr (blue line) and ~405 kyr (red line); (e) Astronomically tuned Log MS series (purple line). The major Oceanic Anoxic Event 1b sub-events are highlighted in light gray.

corroborating the 113.2 Ma age of GTS2020 (Gale et al., 2020). If we used FO of *M. renilaevis* as marker for the Aptian-Albian boundary (e.g., Gradstein et al., 2020; Kennedy et al., 2014), we extrapolated an age of 113.36 Ma. However, to facilitate global correlations (oceans and continental sections) and avoid bioevents diachronism, we suggest adopting the **κ** carbon isotope as an alternative and visual marker of the Aptian-Albian boundary.

Our FATS matches well with absolute ages (Bornemann et al., 2023; Herrle et al., 2015; Selby et al., 2009) and carbon isotope stratigraphy of the PLG core and Vocontian Basin (Coccioni et al., 2014; Herrle et al., 2004). We have been able to define a time span of 2.76 Myr for the OAE 1b event meant, from the 113/Jacob to the Leenhardt Levels (Matsumoto et al., 2020). For individual sub-events, we obtain the following ages 114.07 ± 0.12 Ma for 113/Jacob, 113.28 ± 0.12 Ma for Kilian, 112.49 ± 0.12 Ma for the middle part of the Monte Nerone cluster, 111.70 ± 0.12 Ma for Urbino and 111.28 ± 0.12 Ma for Leenhardt Levels (Table 3). The estimated timespan of the 113/Jacob black-shale is quite like previous studies (Table 4). As this study is the first to provide a timespan of the Monte Nerone, Urbino, and Leenhardt Levels in the UMB, there is no other reference to compare our estimates.

Table 3
Estimated Ages of the Black-Shale Levels

Work	Black-shale levels (estimated age in Ma)				
	113/Jacob	Kilian	M. Nerone	Urbino	Leenhardt
Huang et al., 2010	114.2	112			
Coccioni et al., 2014	113.2	111.5		109.8	>109.2
Sabatino et al., 2018	115.0	112.8		111.3	>110.7
Leandro et al., 2022	113.7	112.9			
Matsumoto et al., 2020	114.5	112.8		111.1	110.5
Fauth et al., 2022		113.6			
Charbonnier et al., 2023	114.0	113.2			
This work	114.06	113.21	112.17	111.67	111.40
	114.07	113.24	112.49	111.69	111.42
	114.08	113.27	112.81	111.71	111.44

4.2. C-Isotope Stages, Their Markers, and Sub-Events Levels Correlations in Different Basins

The PLG site, where the PLG core was drilled, provides one of the most continuous, complete, and best-preserved Aptian-Albian record and is represented by calcareous pelagic rocks extending from the Albian-Cenomanian boundary down to the uppermost Barremian (Coccioni et al., 2012). Several carbon-isotope excursions are observed in the $\delta^{13}C$ record of the PLG core (Coccioni et al., 2014; Leandro et al., 2022) and have a potential for long distance correlations. In this work, we recognize significant landmarks (notable features separating the stages or within these stages), named here as C-markers, which have been observed in other records. We reviewed eight C-isotope stages around the OAE 1b interval, based on the correlation with other sections (Figure 11). This procedure allows us to transpose the ages of significant landmarks of carbon isotope ratios, and then attribute an age to each marker and C-isotope stage.

We obtained the following ages of C-isotope stages, in stratigraphic order: **θ** = ~114.15 ± 0.12 Ma; **ι** = ~113.41 ± 0.12 Ma; **κ** = ~113.32 ± 0.12 Ma; **λ** = ~113.28 ± 0.12 Ma; **μ** = ~113.20 ± 0.12 Ma; **ν** = ~112.30 ± 0.12 Ma; **ξ** = ~111.85 ± 0.12 Ma and **ο** = ~111.50 ± 0.12 Ma (Figure 11). According to these ages we suggest that the following levels can be correlated with respective counterparts in the Vocontian Basin: the Jacob/113 could be related with DC 2, the Monte Nerone Level with the HN2-HN7, and the Urbino Level with the HN13-HN15 (Figure 11). Ba/Al and Mn/Al ratios along the PLG section show two distinct peaks in the Urbino/Paquier interval (Sabatino et al., 2015). The first peak represents the expression of Paquier in the PLG, while the second coincides with the Urbino Level, highlighting the presence of a pair of events associated with the landmark **ξ**.

Carbon-isotope excursions and/or organic rich-levels that define the OAE 1b have been recognized in the Tethyan and North Atlantic regions (e.g., Coccioni et al., 2014; Herrle et al., 2004, 2010, 2015; Kennedy et al., 2014; Trabucho Alexandre et al., 2011). In the Vocontian Basin, four organic-rich levels named Jacob, Kilian, Paquier,

Table 4
Estimated Timespan of Upper Aptian/Lower Albian Organic-Rich Levels

Work	Timespan (kyr)				
	113/Jacob	Kilian	M. Nerone	Urbino	Leenhardt
Huang et al., 2010	~40	~120			
Coccioni et al., 2014		~200			
Leandro et al., 2022	~30	~90			
Fauth et al., 2022		~200			
Charbonnier et al., 2023	~25	~32			
This work	~20	~70	~630	~90	~80

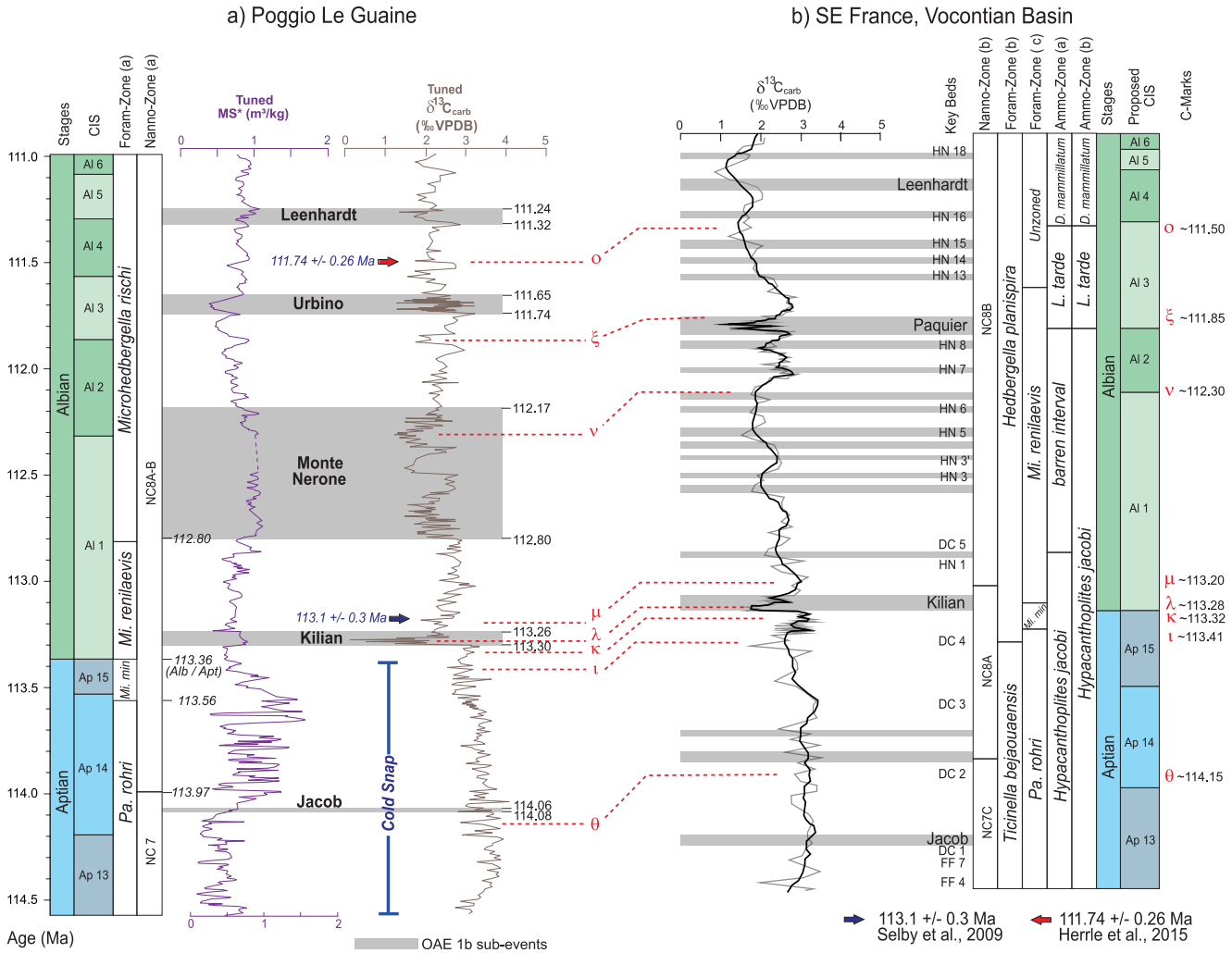

Figure 11. Correlation of upper Aptian-lower Albian intervals in the Umbria-Marche Basin (Poggio le Guaine (PLG) core, on the left) with the Vocontian Basin (on the right) through $\delta^{13}C_{carb}$ records, C-isotope stages and associated markers: (a) PLG foraminiferal and nannofossil zones from Coccioni et al. (2014); (b) Foraminiferal and nannofossil zones from Herrle et al. (2004); (b, c) Foraminiferal zone and ammonite zone from Charbonnier et al. (2023) and (a) Ammonite zone from Bodin et al. (2023). The error in ages is estimated at approximately ~120 kyr.

and Leenhardt (Bréhéret, 1994) have been considered records of the OAE 1b, although some studies consider only the Jacob, Kilian, and Paquier (Trabucho Alexandre et al., 2011) or just the Paquier (Herrle et al., 2004). The internal markers within the C-isotope stages recognized here can be used as reference to make correlations of the OAE 1b interval worldwide. The C-isotope fluctuations could result from the balance between several processes recycling carbon on the Earth's surface, including the input of isotopically light volcanic CO_2, the increased recycling rates of ^{12}C-rich intermediate water, the intensified flux of ^{12}C-rich riverine dissolved inorganic carbon, and the thermal dissociation of methane hydrates (e.g., Bralower et al., 1999; Matsumoto et al., 2020, 2021; Menegatti et al., 1998; Weissert, 1989).

The combined isotope stratigraphy of PLG, Vocontian Basin, DSDP Site 545, and ODP Hole 1049C records (Coccioni et al., 2014) allows us to characterize the studied interval on global scale. The new C-isotope correlation allows us to precisely calibrate the absolute age (111.74 ± 0.26 Ma for **ο** marker) to be transposed into the PLG record and used as a tie-point for a new cyclostratigraphic tuning of entire studied interval. Previous studies used $^{206}Pb/^{238}U$ age of 113.1 ± 0.3 Ma determined for chemically abraded zircon from a tuff horizon 65 cm above the Aptian/Albian boundary (Selby et al., 2009) as a tie-point for the 405 kyr cycles tuning, but the tuff horizon near top *H. jacobi* ammonite zone in the Schwicheldt Ton Member, Gault Formation (Vöhrum, Germany) was ~1,000 km distant from the PLG site. Furthermore, the very top of this ammonite zone has been reported in

different positions (Bodin et al., 2023; Charbonnier et al., 2023; Herrle et al., 2010) and could not be correlated with a specific C-isotope stage. The top of the *H. jacobi* zone is not the best anchoring point for cyclostratigraphic studies, as it has an unconstrained age and thus cannot be correlated with the Kilian Level (Bodin et al., 2023); the Paquier Level (Herrle et al., 2010) and the Leenhardt Level (Charbonnier et al., 2023), Figure 11.

Bornemann et al. (2023) presented the first high-resolution carbon isotope stratigraphy (CIS) for the Berriasian to Coniacian interval from NW Germany that stratigraphically locates the position of the Vöhrum boundary tuff (**μ** marker) in a carbon isotope curve and proposed a slightly older age for the Aptian–Albian boundary of ca. 113.36 Ma. This estimate of the Kilian age (**λ** marker) was anchored on the cyclostratigraphic study of Nebe (1999), which provided a sedimentation rate of 3.6 cm/kyr and extended upwards 20 m of section (interval between tuff and Kilian) to conclude that the Kilian event is 555 ± 13 kyr older than the tuff. As the tuff horizon was dated at 113.1 ± 0.3 Ma (Selby et al., 2009), then the Kilian must have an age of 113.66 ± 0.3 Ma.

We conclude that transposing the **o** marker to the 111.74 ± 0.26 Ma age and test the range of possible ages of the **μ** marker is more realistic and reliable than transposing the top of the *H. jacobi* zone found in Vöhrum as marker of the Aptian-Albian boundary (Gale et al., 2020). Even at a great distance and with the absence of bioevents common to both basins, the CIS provides: (a) the association of 111.74 ± 0.26 Ma age (**o** marker) obtained in Axel Heiberg (Herrle et al., 2015) to the OAE 1b event described on Gale et al. (2020), understood here as a correlation to the Urbino/Paquier at the UMB (Coccioni et al., 2012, 2014; Sabatino et al., 2015, 2018); (b) the association of tuff horizon position (**μ** marker) at the end of the **λ** excursion as 113.1 ± 0.3 Ma (Selby et al., 2009) and; (c) the association of 113.66 ± 0.3 Ma for the Kilian (***k*** marker).

As discussed previously, the 405-kyr cycle remains stable throughout the Phanerozoic, serving as a temporal metric even amidst the chaotic motion of the Solar System (Laskar, 2020). Even for periods prior to 50 Ma, where precise orbital-insolation time series cannot be determined (Laskar et al., 2004), the 405 kyr signal can be used as a temporal metric (Kodama & Hinnov, 2015; Laskar, Fienga, et al., 2011). The stability of this frequency is such that the phase drift over 250 Ma is approximately 405 ka (~1.6‰), much smaller than any radioisotopic dating. As the error range associated with the Vöhrum tuff (113.1 ± 0.3 Ma; Selby et al., 2009) is relatively narrow, being completely encompassed within a 405-kyr cycle, future absolute dating on the Vöhrum tuff aimed at refining this error range will not affect the phase of the signal (Figure 9). However, new absolute dating within the context of the PLG (such as Re-Os) could result in a constant shift along the section without affecting the duration of OAE 1b and its sub-events, since our section is anchored in the temporal metric imposed by the 405-kyr metronome.

The PLG represents one of the most continuous and complete records of OAE 1b (Coccioni et al., 2012), and possible errors related to hiatus in the preserved orbital record (Meyers & Sageman, 2007) are minimized, resulting in minimal signal distortion associated with the propagation of the Milankovitch orbital insolation signal. Additionally, the core drilled at PLG, where the best-preserved Aptian-Albian succession is found, represents a continuous record of fossiliferous pelagic rocks (ideal for cyclostratigraphic studies) extending from the Albian-Cenomanian boundary down to the Barremian (Coccioni et al., 2012; Savian et al., 2016).

The presence of four prominent peaks (instead of the two peaks associated with the combination of the 131/124 kyr and 99/95 kyr signals (Hinnov & Hilgen, 2012)) within the short-eccentricity band may arise from fluctuating sedimentation rates across the analyzed interval or potentially indicate one or more unresolved hiatuses. However, this proposition is refuted by the uninterrupted continuity of the record, as noted by Coccioni et al. (2012, 2014). The overall lower r^2_{opt} of the PLG core reflects the sum of several factors, from gradual variations in sedimentation rates, issues related to the fidelity of the MS proxy, to the presence of various condensed sections (black shales) generating rapid variations in sedimentation rates. The sampling density conducted for this stratigraphic study has a Nyquist Frequency that is completely satisfactory for the full identification of Milankovitch cycles. Theoretical cyclostratigraphic problems related to the quality and absence of rock records, as well as aliasing and sporadic short-term events (such as lava layers or turbidites), are not present in the PLG core.

4.3. Paleoclimate During OAE 1b Event

Paleoceanographic changes during the OAE 1b show that each level enriched in organic matter has its own characteristics, with distinct detrital input values, different types of organic matter, and varying degrees of anoxia

Table 5
Synthesis of Organic Matter-Rich Levels Paleoceanographic Proxies' Indicators

	Detrital input proxies		Volcanism indicators			Productivity		
OAE 1b sub-event	Org. matter–Type (b.)	Fe, Ti (a.)	$^{187}Os/^{186}Os$ (c.)	Hg/TOC (d.)	Plag. Ages (e.)	HI values (b.)	Aeolian (b.)	Ba content (a.)
Jacob	II (mar. contrib.) and III	Low	Yes	at the onset	Yes	High	Yes	Median
Kilian	III and IV (terrestrial)	High	at the onset	at the onset	Yes	Low	Yes (top)	High (onset)
M. Nerone	III and IV (terrestrial)	sporadic	No	sporadic	Yes	Low		High
Urbino/Paquier	II (marine contrib.)	No	No	No	Yes	High		High
Leenhardt	III and IV (terrestrial)	High	No	at the onset	at the onset	Low		Median (onset)

Note. a = This study; b = Sabatino et al., 2015; c = Matsumoto et al., 2022; d = Sabatino et al., 2018; e = Davidson et al., 2023.

and productivity (Bodin et al., 2023; Erbacher et al., 1999; Heimhofer et al., 2006; Matsumoto et al., 2022; Sabatino et al., 2015, 2018). Likely, different geological processes controlled the depositions of the black shales, resulting in a wide range of variables and forcing possibilities (Table 5). However, the long-lasting interval encompassing this highly variable period, often simplified by combining and labeling distinct events under the acronym OAE 1b, prompts us to consider potential explanations. These include: a volcanic origin background of Kerguelen Plateau, Broken Ridge and/or OJP (Davidson et al., 2023; Frey et al., 2000; Sabatino et al., 2015; Whitechurch et al., 1992) or a long-term orbital cycle (longer than 2 Myr) or even the effect of orbital chaotic resonance (Ma et al., 2017).

Sabatino et al. (2015) concluded that the enhanced burial of barium in the latest Aptian–early Albian could reflect higher marine primary productivity, which is presumably driven by higher atmospheric pCO_2, enhanced terrestrial weathering and additional nutrient delivery to the ocean. They suggested that the negative excursions in the $\delta^{13}C_{carb}$ in the Kilian and Urbino/Paquier Levels could be related to a major contribution of isotopically light terrestrial carbonate ions by an enhanced continental runoff during more humid conditions, as clearly testified by the detrital proxies (Sabatino et al., 2015).

The PLG Aptian-Albian sediments were deposited during an exceptionally warm climate (Sabatino et al., 2015), with short term cold episodes (Bodin et al., 2023; Bottini et al., 2015; Herrle et al., 2015; McAnena et al., 2013). Some pieces of evidence such as glendonites, glacial tillites and dropstones support the existence of short-term glacial intervals (Price, 1999). Our correlation based on C-isotope positions **of the** *Glendonites beds* of AHI (Herrle et al., 2015) and the concurrent Cold Snap event (McAnena et al., 2013) at the PLG support the existence of cool shelf waters during late Aptian age. The basal interval of studied section of the PLG, described as Cold Snap (Bottini et al., 2015; Leandro et al., 2022; McAnena et al., 2013), is dominated by the lowest levels of titanium until the planktonic foraminiferal turnover.

The rise in titanium levels after the Cold Snap suggests that the temperature increase (temperature index; Bottini & Erba, 2018) was likely accompanied by increased continental weathering and a greater continental input of Ti. The three eCOCO maps (MS, Ti, and Fe series; Figures 4 and 6) show sedimentation rates with a slight increase after the end of the Cold snap (McAnena et al., 2013), likely related to the return and/or amplification of terrigenous influxes associated with the return to the typical "warm and humid" Cretaceous pattern, from the stratigraphic level of ~65 m. This return to pre-Cold snap conditions is also evident through carbon isotope data, which gradually (linear trend) tend toward lower $\delta^{13}C$ values.

It is noteworthy that there is a mismatch between the peaks of Hg/TOC and levels enriched in organic matter (Sabatino et al., 2018). Additionally, the peaks of volcanism associated with the OAE 1b event occur only in the initial portion of the event, with a non-volcanic character being attributed to the majority of OEA 1b (Matsumoto et al., 2022). This suggests that volcanism (and the extreme climatic conditions associated with these events) are not the cause of the deposition of these levels but rather an amplifying component of the orbital forcing that conditioned the generation of intense monsoon events and high weathering, as supported by the relationship between some enriched levels and weathering proxies. These arguments lead us to agree with the "multiple drivers" mechanism proposed by Wang et al. (2022) for atmospheric-circulation reorganization.

In the PLG core series, the $CaCO_3$ curve follows a long cycle with an inverse trend with respect to MS. Except from the Urbino/Paquier interval, all black shales are depleted in $CaCO_3$ reflecting fluctuations in carbonate productivity and terrigenous sediment supply. Between the Jacob Level and the planktonic foraminiferal turnover, there is an interval with high values of $CaCO_3$ and MS that could be ascribed to a deposition in a different environmental context (higher level of MS associated with high $CaCO_3$ content, a feature opposite to the entire rest of the studied interval), relative to the climax of the Cold Snap event (e.g., Bottini et al., 2015; Leandro et al., 2022; McAnena et al., 2013) and abnormally enriched with Mn/Al (Sabatino et al., 2015). This oscillation of ∼0.5 Myr in the $CaCO_3$ data is related to an increase of MS and indicates a paleoclimatic control that changes the total amount of magnetic particles or the magnetic carrier. A notable feature is the presence of high orders cycles in the $CaCO_3$ data, likely associated with episodes of enhanced carbonate dissolution (Broecker & Clark, 1999).

The Ti and Fe contents are inferred here as proxies for arid and humid phases. The relationship between the phases of the signals of MS, Fe, Ti, and $CaCO_3$ suggests a common paleoclimatic control, where the orbital forcing is amplified by stochastic occurrences, corresponding to volcanic episodes and rapid atmospheric CO_2 input (Matsumoto et al., 2020, 2022; Sabatino et al., 2015). Heimhofer et al. (2006), on the basis of a strong increase in terrestrial palynomorphs, interpreted that the beginning of OAE 1b event in the Vocontian Basin as being primarily formed by detrital inputs from the land detrital components. Arid conditions during the late Aptian–early Albian interval with more humid condition in the uppermost Aptian Kilian and early Albian Urbino/Paquier Levels (Sabatino et al., 2015) could be a key to understand the cause (s) for organic-rich levels deposition.

Wavelengths analysis (Figures 3 and 4) suggest three different cycles, with different periods, forcing the paleoclimate: the first one, a long-period wavelength (combination of Myr cycles with 1,600, 1,000 and 700 kyr) with minimal values associated with Cold Snap and Monte Nerone intervals; the second wavelength that provides the alternation of carbonate bundles with black shales could be also observed in the upper section; and a third one with higher frequency, with time durations similar to those observed in the deposition of black shales. The Kilian and Leenhardt Levels are positively correlated with short-term oscillations in both XRF proxies, highlighting that the increased continental sediment input, contributed to the deposition of these lithofacies. On the other hand, no relationship between increased continental input and the 113/Jacob and Urbino/Paquier Levels was found. The long-term variations in Hg/TOC values associated with peaks could document that the effects of significant Hg emissions are related to the multi-phase emplacement of volcanism during the Aptian-early Albian (Sabatino et al., 2018), is probably the responsible for the termination of the arid and relatively cool conditions of the Cold Snap (McAnena et al., 2013; Wang et al., 2022).

A synthesis of studies related to the organic-enriched levels that are part of OAE 1b highlights the various mechanisms and forcings responsible for the deposition of these levels (Table 5). The variables indicate that the Jacob/113 sub-event is clearly a "volcanic" event that resulted in high productivity, as shown by volcanic indicators and the absence of weathering indicators. Pyrolysis analyses reveal that the Jacob Level is composed of continental-origin organic matter in the Vocontian Basin (Bodin et al., 2023). However, in the PLG, a significant marine contribution is present (Sabatino et al., 2015), highlighting paleogeographic control.

The Kilian sub-event presents a mixed character (volcanic + monsoonal), as both the presence of continental organic matter and precursor eruptions, along with the ages of preferential plagioclases, suggest that its deposition must have been conditioned by both the induced effect of volcanic activity and the result of changes in Hadley circulation dynamics. This forced large-scale precipitation and stratification of the water column, marking the end of the Cold Snap period. In contrast to the Jacob sub-event, the organic matter present in the Kilian Level is of continental origin in the PLG. However, in the Vocontian Basin (Briers section), it exhibits a substantial marine content with increased primary productivity (Bodin et al., 2023). The cluster related to the Monte Nerone interval is very enigmatic and seems to have a mixed character. The sediments become more reddish and argillaceous, giving this interval a CORB-like characteristic (Coccioni et al., 2014; Wang et al., 2009). The high frequency of lithological intercalation, associated with sporadic inputs of terrestrial material, suggests a monsoonal character. However, the lack of correlation between volcanic indicators does not allow for a perfect characterization of this interval as volcanic.

Despite the suggestion of a possible disconnection between the Urbino and Paquier Levels, and the subdivision of the Paquier Level into two events (Erbacher et al., 1999; Kuypers et al., 2002), we will treat them as comparable intervals for now. The clear marine contribution, evidenced by the presence of marine planktonic *archaea*, high productivity, extreme redox conditions (presence of redox-sensitive elements), very high thallium isotope values (Wang et al., 2022), and the absence of volcanic indicators would result in a characterization of this level as an example of a monsoonal global anoxic event. However, the lack of detrital input indicators suggests that the Paquier Level is likely associated with a major transgressive event, unlike the Leenhardt Level, which is characterized as a clearly monsoonal event (terrestrial organic matter and high values of proxies related to weathering and humidity), combined with a volcanic event, as shown by volcanic indicators, as in Table 5.

We conclude that the Cold Snap period, characterized by milder temperatures compared to the average of the Cretaceous period, comes to an end due to the input of volcanic CO_2 resulting from the implementation of LIPs, initiating a period of hyperthermia, heavy precipitation, intense weathering and marine primary productivity. The significant input of continental material resulting from weathering conditioned the deposition of organic-rich levels during the OAE 1b event. In chaos theory, the effect where a small change in one variable can cause significant and amplified changes in other variables is known as the "butterfly effect." Large volcanic eruptions likely played this role in paleoclimate during OAE 1b, acting as "stochastic noise" in the nonlinear paleoclimatic dynamic system. Rapid marine transgressions and atmospheric disturbances related to these peaks of volcanism served as amplifiers of orbital forcings, resulting in deoxygenation and carbon burial events deposited during OAE 1b.

5. Conclusions

A cyclostratigraphic analysis was performed on the MS, Ti and Fe series of the upper Aptian-lower Albian interval from the PLG core, encompassing the pelagic Marne a Fucoidi succession of the Umbria-Marche Basin (Central Italy), which is one of the most detailed sedimentary records of this period. The new temporal calibration through the metric imposed by orbital cycles allows us to better correlate the paleoceanographic fluctuations within the OAE 1b interval with their respective forcings. Based on these, we provide evidence of:

1. The MS, Ti, and Fe data sets display a strong 405-kyr cycle signal that correlates with the long-eccentricity Milankovitch cycle. Our interpretation is supported by SAR statistical tests (TimeOpt and COCO/eCOCO methodologies), resulting in an average sediment accumulation rate (SAR) of 0.5 cm/kyr. The Ti and Fe profiles reveal clear control of SAR by weathering and terrigenous input.
2. By combining new biostratigraphic and high-resolution isotopic data, a 405-kyr calibrated floating astronomical timescale was constructed for the PLG core, and we can infer an age of ∼113.56 ± 0.12 Ma for the FO of *M. miniglobularis*, ∼113.36 ± 0.12 Ma for the FO of *M. renilaevis* and ∼112.80 ± 0.12 Ma for the FO of *M. rischi.*
3. Our astronomical calibration exhibited ∼7 long eccentricity cycles through the interval between 62.5 and 53.0 m (OAE 1b interval), which covers a timespan of ∼2.84 Myr. The chronostratigraphic study also provides an age of 114.07 ± 0.12 Ma for 113/Jacob 113.28 ± 0.12 Ma for Kilian, 112.49 ± 0.12 Ma as a central age of the Monte Nerone cluster, 111.70 ± 0.12 Ma for Urbino and 111.28 ± 0.12 Ma for Leenhardt sub-events, and a timespan of ∼20 kyr for 113/Jacob, 70 kyr for Kilian, 630 kyr for Monte Nerone cluster, 90 kyr for Urbino and 80 kyr for Leenhardt Levels.
4. C-isotope stratigraphy shows an immense potential for be used as tiepoint for cyclostratigraphic studies and becomes a valuable way to evaluate diachronism of bioevents, allowing correlation between different basins through c-marks, with ages estimated using PLG core tuning as: **θ** = ∼114.15 ± 0.12 Ma; **ι** = ∼113.41 ± 0.12 Ma; **κ** = ∼113.34 ± 0.12 Ma; **λ** = ∼113.28 ± 0.12 Ma; **μ** = ∼113.20 ± 0.12 Ma; **ν** = ∼112.30 ± 0.12 Ma; **ξ** = ∼111.85 ± 0.12 Ma and **ο** = ∼111.50 ± 0.12 Ma, suggesting that: Jacob/113 PLG Level could be related with DC 2 of Vocontian Basin; Monte Nerone PLG Level with HN2-HN7 Vocontian Basin Levels and; Urbino PLG Level with HN14-HN15 Vocontian Basin Levels.
5. Each sub-event within the OAE 1b event exhibits distinct characteristics arising from the interplay of a warm climate induced by volcanic CO_2 input (which acts as an amplifier of orbital forcings, driving paleoclimate changes) and oceanic-atmospheric disturbances such as heavy precipitation and intense weathering. These factors contribute to deoxygenation and carbon burial during the OAE 1b period.

Data Availability Statement

Data sets from PLG core were generated in this study. New data are archived in the Zenodo database (Ramos, 2024).

Acknowledgments

The paper is an integral part of the Project: *Processamento e interpretação de dados magnetoestratigráficos do Cretáceo das Bacias Brasileiras*, which is financially supported by Petróleo Brasileiro S.A.—Petrobras (FAURGS 8368). J.M.F. RAMOS acknowledges Petrobras for PhD process. J.F.S also acknowledges the *Fundação de Amparo à Pesquisa do Estado do Rio Grande do Sul* (FAPERGS) (Grant 16/2551-0000213-4), and CNPq (Grants 304022/2018-7, 201508/2009-5, 427280/2018-4, 311231/2021-7). D.R.F. thanks the Foundation Carlos Chagas Filho Research Support of the State of Rio de Janeiro (FAPERJ–Grant E-26/200.931/2022) and CNPq (Grant 314462/2020-1). M. Giorgioni thanks CNPq (processo n. 307158/2020-9). This study was financed in part by the Coordenação de Aperfeiçoamento de Pessoal de Nível Superior - Brasil (CAPES) - Finance Code 001. The authors thank Hironao Matsumoto for his corrections and suggestions throughout the paper. The authors are grateful for the suggestions and comments from the Editor and the reviewers.

References

Ait-Itto, F.-Z., Martinez, M., Deconinck, J. F., & Bodin, S. (2023). Astronomical calibration of the OAE1b from the Col de Pré-Guittard section (Aptian-Albian), Vocontian Basin, France. *Cretaceous Research*, *150*, 105618. https://doi.org/10.1016/j.cretres.2023.105618

Arthur, M. A., Jenkyns, H. C., Brumsack, H. J., & Schlanger, S. O. (1990). Stratigraphy, geochemistry, and Paleoceanography of organic carbon-rich cretaceous sequences. In R. N. Ginsburg & B. Beaudoin (Eds.), *Cretaceous Resources, events and rhythms* (pp. 75–119). Kluwer.

Arthur, M. A., & Premoli Silva, I. (1982). Development of widespread organic carbon-rich strata in the Mediterranean Tethys. In S. O. Schlanger & M. B. Cita (Eds.), *Nature of cretaceous carbon-rich facies* (pp. 7–54). Academic.

Arz, H. W., Patzold, J., & Wefer, G. (1998). Correlated millennial scale changes in surface hydrography and terrigenous sediment yield inferred from last glacial marine deposits off northeastern Brazil. *Quaternary Research*, *50*(2), 157–166. https://doi.org/10.1006/qres.1998.1992

Bodin, S., Charpentier, M., Ullmann, C. V., Rudra, A., & Sanei, H. (2023). Carbon cycle during the late Aptian–early Albian OAE 1b: A focus on the Kilian–Paquier levels interval. *Global and Planetary Change*, *222*, 104074. https://doi.org/10.1016/j.gloplacha.2023.104074

Bornemann, A., Erbacher, J., Blumenberg, M., & Voigt, S. (2023). A first high-resolution carbon isotope stratigraphy from the boreal (NW Germany) for the Berriasian to Coniacian interval—Implications for the timing of the Aptian–Albian boundary. Front. *Earth Sciences*, *11*, 1173319. https://doi.org/10.3389/feart.2023.1173319

Bottini, C., & Erba, E. (2018). Mid-Cretaceous paleoenvironmental changes in the western Tethys. *Climate of the Past*, *14*(8), 1147–1163. https://doi.org/10.5194/cp-14-1147-2018

Bottini, C., Erba, E., Tiraboschi, D., Jenkyns, H. C., Schouten, S., & Sinninghe Damsté, J. S. (2015). Climate variability and ocean fertility during the Aptian Stage. *Climate of the Past*, *11*(3), 383–402. https://doi.org/10.5194/cp-11-383-2015

Bralower, T. J., Cobabe, E., Clement, B., Sliter, W. V., Osburn, C., & Longoria, J. (1999). The record of global change in mid-Cretaceous (Barremian-Albian) sections from the Sierra Madre, northeastern Mexico. *Journal of Foraminiferal Research*, *29*(4), 418–437.

Bréhéret, J.-G. (1983). Sur des niveaux de black shales dans l'Albien inférieur et moyen du domaine vocontien (SE de la France): étude de nannofaciès et signification des paléoenvironnements. *Bulletin du Muséum National d'Histoire Naturelle. Paris*, *5*(1), 113–159.

Bréhéret, J.-G. (1988). Episodes de sédimentation riche en matière organique dans les marnes bleues d'âge aptien et albien de la partie pélagique du bassin vocontien. *Bulletin de la Societe Geologique de France*, *8*(4), 349–356. https://doi.org/10.2113/gssgfbull.iv.2.349

Bréhéret, J. G. (1994). The mid-cretaceous organic-rich sediments from the Vocontian zone of the French southeast basin. In A. Mascle (Ed.), *Hydrocarbon and petroleum geology of France. Special publication of the European association of petroleum geoscientists No. 4* (pp. 295–320). Springer.

Broecker, W. S., & Clark, E. (1999). $CaCO_3$ size distribution: A paleocarbonate ion proxy. *Paleoceanography*, *14*(5), 596–604. https://doi.org/10.1029/1999pa900016

Browning, E. L., & Watkins, D. K. (2008). Elevated primary productivity of calcareous nannoplankton associated with ocean Anxoic event 1b during the Aptian/Albian transition (early cretaceous). *Papers in the Earth and Atmospheric Sciences*, *237*. Retrieved from https://digitalcommons.unl.edu/geosciencefacpub/237

Chambers, L. M., Pringle, M. S., & Fitton, J. G. (2004). Phreatomagmatic eruptions on the Ontong Java Plateau: An Aptian 40Ar/39Ar age for volcaniclastic rocks at ODP site 1184. In G. Fitton, J. Mahoney, P. Wallace, & A. Saunders (Eds.), *Origin and evolution of the Ontong Java Plateau*. Geological Society, London, Special Publication (Vol. 229(1), pp. 325–331). https://doi.org/10.1144/GSL.SP.2004.229.01.18

Channell, J. E. T., D'Argenio, B., & Horvath, F. (1979). Adria, the African promontory, in Mesozoic Mediterranean paleogeography. *Earth-Science Reviews*, *15*, 213–292.

Charbonnier, G., Boulila, S., Spangenberg, J. E., Adatte, T., Föllmi, K. B., & Laskar, J. (2023). Astrochronology of the Aptian stage and evidence for the chaotic orbital motion of Mercury. *Earth and Planetary Science Letters*, *610*, 118104. https://doi.org/10.1016/j.epsl.2023.118104

Coccioni, R. (1996). The cretaceous of the Umbria-Marche Apennines (Central Italy). *Jost Wiedmann Symposium on Cretaceous Stratigraphy, Paleobiology and Paleobiogeography, Tübingen*, 7–10.

Coccioni, R. (2001). The "Pialli level" from the latest Albian of the Umbria-Marche Apennines (Italy). *Federazione Italiana di Scienze della Terra, Geoitalia*, *2001*, 192–193.

Coccioni, R., Erba, E., & Premoli Silva, I. (1992). Barremian-Aptian calcareous plankton biostratigraphy from the Gorgo a Cerbara section (Marche, Central Italy) and implications for plankton evolution. *Cretaceous Research*, *13*, 517–537. https://doi.org/10.1016/0195-6671(92)90015-I

Coccioni, R., Franchi, R., Nesci, O., Perilli, N., Wezel, F. C., & Battistini, F. (1990). Stratigrafia, micropaleontologia e mineralogía delle Marne a Fucoidi delle sezioni di Poggio le Guaine e del Fiume Bosso (Appennino umbro-marchigiano). Atti 2° Convegno Internazionale "Fossili, Evoluzione, Ambiente", Pergola, 25–30 ottobre 1987, Tecnostampa (pp. 163–201).

Coccioni, R., Franchi, R., Nesci, O., Wezel, F. C., Battistini, F., & Pallecchi, P. (1989). Stratigraphy and mineralogy of the Selli level (early Aptian) at the base of the Marne a Fucoidi in the Umbro-Marchean Apennines, Italy. In J. Wiedmann (Ed.), *Cretaceous of the western Tethys. Proceedings 3rd international cretaceous symposium* (pp. 563–584). E. Schweizerbart'sche Verlagsbuchhandlung.

Coccioni, R., Jovane, L., Bancalà, G., Bucci, C., Fauth, G., Frontalini, F., et al. (2012). Umbria-Marche Basin, Central Italy: A reference section for the Aptian-Albian interval at low latitudes. *Scientific Drilling*, *13*(13). https://doi.org/10.2204/iodp.sd.13.07.2011

Coccioni, R., Nesci, O., Tramontana, M., Wezel, F. C., & Moretti, E. (1987). Descrizione di un livello–guida "radiolaritico-bituminoso-ittiolitico" alla base delle Marne a Fucoidi nell'Appennino umbro-marchigiano. *Bollettino della Società geologica italiana*, *106*, 183–192.

Coccioni, R., Sabatino, N., Frontalini, F., Gardin, S., Sideri, M., & Sprovieri, M. (2014). The neglected history of Oceanic Anoxic Event 1b: Insights and new data from the Poggio le Guaine section (Umbria–Marche Basin). *Stratigraphy*, *11*(3–4), 245–282. https://doi.org/10.29041/strat.11.3.03

Davidson, P. C., Koppers, A. A. P. K., Sano, T., & Hanyu, T. (2023). A younger and protracted emplacement of the Ontong Java Plateau. *Science*, *380*(6650), 1185–1188. https://doi.org/10.1126/science.ade8666

Eldholm, O., & Coffin, M. F. (2000). Large igneous province and plate tectonics. The Hystory and dynamics of global plate motions. *Geophysical Monograph Series*, *121*.

Erbacher, J., Hemleben, C., Huber, B. T., & Markey, M. (1999). Correlating environmental changes during early Albian oceanic anoxic event 1B using benthic foraminiferal paleoecology. *Marine Micropaleontology*, *38*(1), 7–28. https://doi.org/10.1016/S0377-8398(99)00036-5

Fauth, G., Krahl, G., Kochhann, K. G. D., Bom, M. H., Fauth, S. B., Bruno, M. D. R., et al. (2022). Astronomical calibration of the latest Aptian to middle Albian in the South Atlantic Ocean (Sergipe-Alagoas basin, Brazil). *Palaeogeography, Palaeoclimatology, Palaeoecology*, *602*, 111175. https://doi.org/10.1016/j.palaeo.2022.111175

Frey, F. A., Coffin, M. F., Wallace, P. J., Weis, D., Zhao, X., Wise Jr, S. W., et al. (2000). Origin and evolution of a submarine large igneous province: The Kerguelen Plateau and Broken Ridge, southern Indian Ocean. *Earth and Planetary Science Letters*, *176*(1), 73–89. https://doi.org/10.1016/s0012-821x(99)00315-5

Gale, A. S., Mutterlose, J., Batenburg, S., Gradstein, F. M., Agterberg, F. P., Ogg, J. G., & Petrizzo, M. R. (2020). The Cretaceous period. In *Geologic time scale 2020* (pp. 1023–1086). Elsevier. https://doi.org/10.1016/B978-0-12-824360-2.00027-9

Gradstein, F. M., Ogg, J. G., Schmitz, M., & Ogg, G. (2020). *The geologic time scale 2020*. Elsevier.1390.

Grippo, A., Fischer, A. G., Hinnov, L. A., Herbert, T. D., & Premoli-Silva, I. (2004). Cyclostratigraphy and chronology of the Albian stage (Piobbico core, Italy). *Cyclostratigraphy: approaches and case histories*, *81*, 57–81.

Heimhofer, U., Hochuli, P. A., Herrle, J. O., & Weissert, H. (2006). Contrasting origins of early cretaceous black shales in the Vocontian Basin: Evidence from palynological and calcareous nannofossil records. *Palaeogeography, Palaeoclimatology, Palaeoecology*, *235*(1–3), 93–109. https://doi.org/10.1016/j.palaeo.2005.09.025

Herbert, T. D., & Fischer, A. G. (1986). Milankovitch climatic origin of mid-Cretaceous black shale rhythms in central Italy. *Nature*, *321*, 739–743. https://doi.org/10.1038/321739a0

Herrle, J. O., Kössler, P., & Bollmann, J. (2010). Palaeoceanographic differences of early Late Aptian black shale events in the Vocontian Basin (SE France). *Palaeogeography, Palaeoclimatology, Palaeoecology*, *297*(2), 367–376. https://doi.org/10.1016/j.palaeo.2010.08.015

Herrle, J. O., Kössler, P., Friedrich, O., Erlenkeuser, H., & Hemleben, C. (2004). High-resolution carbon isotope records of the Aptian to lower Albian from SE France and the Mazagan Plateau (DSDP site 545): A stratigraphic tool for paleoceanographic and paleobiologic reconstruction. *Earth and Planetary Science Letters*, *218*(1–2), 149–161. https://doi.org/10.1016/S0012-821X(03)00646-0

Herrle, J. O., Schröder-Adams, C. J., Davis, W., Pugh, A. T., Galloway, J. M., & Fath, J. (2015). Mid-cretaceous High Arctic stratigraphy, climate, and oceanic anoxic events. *Geology*, *43*(5), 403–406. https://doi.org/10.1130/G36439.1

Hinnov, L., & Hilgen, F. J. (2012). Cyclostratigraphy and astrochronology. In F. M. Grandstein, J. G. Ogg, M. D. Schmitz, & G. E. Ogg (Eds.), *The geologic time scale 2012* (pp. 63–78). Elsevier.

Huang, C., Hinnov, L. A., Fischer, A. G., Grippo, A., & Herbert, T. (2010). Astronomical tuning of the Aptian stage from Italian reference sections. *Geology*, *238*(10), 899–903. https://doi.org/10.1130/g31177.1

Huber, B. T., & Leckie, M. R. (2011). Planktic foraminiferal species turnover across deep-sea Aptian/Albian Boundary sections. *Journal of Foraminiferal Research*, *41*(1), 53–95. https://doi.org/10.2113/gsjfr.41.1.53

Jenkyns, H. C. (2010). Geochemistry of oceanic anoxic events. *Geochemistry, Geophysics, Geosystems*, *11*(3), Q03004. https://doi.org/10.1029/2009GC002788

Kennedy, W. J., Gale, A. S., Huber, B. T., Petrizzo, M. R., Bown, P., Barchetta, A., & Jenkyns, H. C. (2014). Integrated stratigraphy across the Aptian/Albian boundary at the Col de Pré-Guittard (southeast France): A candidate Global Boundary Stratotype Section. *Cretaceous Research*, *51*, 248–259. https://doi.org/10.1016/j.cretres.2014.06.005

Kennedy, W. J., Gale, A. S., Huber, B. T., Petrizzo, M. R., Bown, P., & Jenkyns, H. C. (2017). The Global Boundary Stratotype Section and Point (GSSP) for the base of the Albian Stage, of the Cretaceous, the Col de Pré-Guittard section, Arnayon, Drôme, France. *Episodes*, *40*(No. 3), 177–188. https://doi.org/10.18814/epiiugs/2017/v40i3/017021

Kodama, K., & Hinnov, L. (2015). Rock magnetic cyclostratigraphy. https://doi.org/10.1002/9781118561294

Kuypers, M. M. M., Blokker, P., Hopmans, E. C., Kinkel, H., Pancost, R. D., Schouten, S., & Sinninghe Damsté, J. S. (2002). Archaeal remains dominate marine organic matter from the early Albian oceanic anoxic event 1b. *Palaeogeography, Palaeoclimatology, Palaeoecology*, *185*(1–2), 211–234. https://doi.org/10.1016/S0031-0182(02)00301-2

Larson, R. L., & Erba, E. (1999). Onset of the mid-Cretaceous greenhouse in the Barremian-Aptian: Igneous events and the biological, sedimentary, and geochemical responses. *Paleoceanography*, *14*(6), 663–678. https://doi.org/10.1029/1999pa900040

Laskar, J. (1989). A numerical experiment on the chaotic behaviour of the solar system. *Nature*, *338*(6212), 237–238. https://doi.org/10.1038/338237a0

Laskar, J. (1990). The chaotic motion of the solar system - A numerical estimate of the size of the chaotic zones. *Icarus*, *88*(2), 266–291. https://doi.org/10.1016/0019-1035(90)90084-m

Laskar, J. (2020). Astrochronology. In *Geologic time scale 2020* (pp. 139–158).

Laskar, J., Fienga, A., Gastineau, M., & Manche, H. (2011). La2010: A new orbital solution for the long-term motion of the Earth. *Astronomy & Astrophysics*, *532*, A89. https://doi.org/10.1051/0004-6361/201116836

Laskar, J., Gastineau, M., Delisle, J., Farrées, A., & Fienga, A. (2011). Strong chaos induced by close encounters with ceres and vesta. *Astronomy and Astrophysics*, *532*, L4. https://doi.org/10.1051/0004-6361/201117504

Laskar, J., Robutel, P., Joutel, F., Gastineau, M., Correia, A. C. M., & Levrard, B. (2004). A long-term numerical solution for the insolation quantities of the Earth. *Astronomy & Astrophysics*, *428*(1), 261–285. https://doi.org/10.1051/0004-6361:20041335

Leandro, C. G., Savian, J. F., Kochhann, M. V. L., Franco, D. R., Coccioni, R., Frontalini, F., et al. (2022). Astronomical tuning of the Aptian stage and its implications for age recalibrations and paleoclimatic events. *Nature Communications*, *13*(1), 2941. https://doi.org/10.1038/s41467-022-30075-3

Leckie, R. M., Bralower, T. J., & Cashman, R. (2002). Oceanic anoxic events and plankton evolution: Biotic response to tectonic forcing during the mid-Cretaceous. *Paleoceanography*, *17*(3), 13-11–13-29. https://doi.org/10.1029/2001PA000623

Li, M., Hinnov, L., & Kump, L. (2019). Acycle: Time-series analysis software for paleoclimate research and education. *Computers & Geosciences*, *127*, 12–22. https://doi.org/10.1016/j.cageo.2019.02.011

Li, M., Kump, L., Hinnov, L., & Mann, M. E. (2018). Tracking variable sedimentation rates and astronomical forcing in Phanerozoic paleoclimate proxy series with evolutionary correlation coefficients and hypothesis testing. *Earth and Planetary Science Letters*, *501*, 165–179. https://doi.org/10.1016/j.epsl.2018.08.041

Liu, W., Wu, H., Hinnov, L. A., Xi, D., He, H., Zhang, S., & Yang, T. (2020). Early cretaceous terrestrial Milankovitch cycles in the Luanping basin, North China and time constraints on early stage Jehol Biota evolution. *Frontiers of Earth Science*, *8*, 178. https://doi.org/10.3389/feart.2020.00178

Ludvigson, G. A., Joeckel, R. M., Gonzalez, L. A., Gulbranson, E. L., Rasbury, E. T., Hunt, G. J., et al. (2010). Correlation of Aptian-Albian Carbon Isotope Excursions in Continental Strata of the Cretaceous Foreland Basin, Eastern Utah, U.S.A. *Journal of Sedimentary Research*, *80*(11), 955–974. https://doi.org/10.2110/jsr.2010.086

Ma, C., Meyers, S. R., & Sageman, B. B. (2017). Theory of chaotic orbital variations confirmed by Cretaceous geological evidence. *Nature*, *542*(7642), 468–470. https://doi.org/10.1038/nature21402

Mann, M. E., & Lees, J. M. (1996). Robust Estimation of Background Noise and Signal Detection in Climatic Time Series. *Climatic Change*, *33*(3), 409–445. https://doi.org/10.1007/bf00142586

Matsumoto, H., Coccioni, R., Frontalini, F., Shirai, K., Jovane, L., Trindade, R., et al. (2022). Mid-cretaceous marine Os isotope evidence for heterogeneous cause of oceanic anoxic events. *Nature Communications*, *13*(1), 239. https://doi.org/10.1038/s41467-021-27817-0

Matsumoto, H., Coccioni, R., Frontalini, F., Shirai, K., Jovane, L., Trindade, R. I. F., et al. (2021). Long-term Aptian marine osmium isotopic record of Ontong Java Nui activity. *Geology*, *49*(9), 1148–1152. https://doi.org/10.1130/G48863.1

Matsumoto, H., Kuroda, J., Coccioni, R., Frontalini, F., Sakai, S., Ogawa, N. O., & Ohkouchi, N. (2020). Marine Os isotopic evidence for multiple volcanic episodes during Cretaceous Oceanic Anoxic Event 1b. *Scientific Reports*, *10*(1), 12601. https://doi.org/10.1038/s41598-020-69505-x

McAnena, A., Flögel, S., Hofmann, P., Herrle, J. O., Griesand, A., Pross, J., et al. (2013). Atlantic cooling associated with a marine biotic crisis during the mid-cretaceous period. *Nature Geoscience*, *6*(7), 558–561. https://doi.org/10.1038/ngeo1850

Menegatti, A. P., Weissert, H., Brown, R. S., Tyson, R. V., Farrimond, P., Strasser, A., & Caron, M. (1998). High-resolution $\delta^{13}C$ stratigraphy through the Early Aptian "Livello selli" of the Alpine tethys. *Paleoceanography*, *13*(5), 530–545. https://doi.org/10.1029/98PA01793

Meyers, S. R. (2014). Astrochron: An R Package for Astrochronology. Retrieved from https://cran.r-project.org/package=astrochron

Meyers, S. R. (2015). The evaluation of eccentricity-related amplitude modulation and bundling in paleoclimate data: An inverse approach for astrochronologic testing and time scale optimization. *Paleoceanography*, *30*(12), 1625–1640. https://doi.org/10.1002/2015PA002850

Meyers, S. R. (2019). Cyclostratigraphy and the problem of astrochronologic testing. *Earth-Science Reviews*, *190*, 190–223. https://doi.org/10.1016/j.earscirev.2018.11.015

Meyers, S. R., & Sageman, B. (2007). Quantification of Deep-Time Orbital Forcing by Average Spectral Misfit. *American Journal of Science*, *307*(5), 773–792. https://doi.org/10.2475/05.2007.01

Meyers, S. R., Sageman, B., & Hinnov, L. (2001). Integrated quantitative stratigraphy of the Cenomanian-Turonian Bridge Creek Limestone Member using evolutive harmonic analysis and stratigraphic modeling. *Journal of Sedimentary Research*, *71*(4), 627–643. https://doi.org/10.1306/012401710628

Nebe, D. W. (1999). *Zyklenuntersuchungen an unterkretazischen Sedimenten in NW-Deutschland - Nachweisbarkeit von Milankovitch-Zyklen*. (Phd thesis). Ruhr-University.

Ogg, J. G., Ogg, G., & Gradstein, F. M. (2016). *A concise geologic time scale: 2016* (p. 234). Elsevier.

Petrizzo, M. R., Huber, B. T., Gale, A. S., Barchetta, A., & Jenkyns, H. C. (2012). Abrupt planktic foraminiferal turnover across the Niveau Kilian at Col de Pré-Guittard (Vocontian Basin, Southeast France): New criteria for defining the Aptian/Albian boundary. *Newsletters on Stratigraphy*, *45*(1), 55–74. https://doi.org/10.1127/0078-0421/2012/0013

Pokorný, J., Suza, P., Pokorný, P., Chlupáčová, M., & Hrouda, F. (2006). Widening power of low-fi eld magnetic methods in the investigation of rocks and environmental materials using the Multi-Function Kappabridge Set. *Geophysical Research Abstracts*, *8*. abs. EGU 06-A-04141.

Price, G. D. (1999). The evidence and implications of polar ice during the Mesozoic. *Earth-Science Reviews*, *48*(3), 183–210. https://doi.org/10.1016/s0012-8252(99)00048-3

Ramos, J. (2024). PLG OAE 1b MS, Fe and Ti data [Dataset]. *Zenodo*. https://doi.org/10.5281/zenodo.10557295

Sabatino, N., Coccioni, R., Manta, D. S., Baudin, F., Vallefuoco, M., Traina, A., & Sprovieri, M. (2015). High-resolution chemostratigraphy of the late Aptian–early Albian oceanic anoxic event (OAE 1b) from the Poggio le Guaine section (Umbria–Marche Basin, central Italy). *Palaeogeography, Palaeoclimatology, Palaeoecology*, *426*, 319–333. https://doi.org/10.1016/j.palaeo.2015.03.009

Sabatino, N., Ferraro, S., Coccioni, R., Bonsignore, M., Del Core, M., Tancredi, V., & Sprovieri, M. (2018). Mercury anomalies in upper Aptian-lower Albian sediments from the Tethys Realm. *Palaeogeography, Palaeoclimatology, Palaeoecology*, *495*, 163–170. https://doi.org/10.1016/j.palaeo.2018.01.008

Savian, J. F., Trindade, R. I. F., Janikian, L., Jovane, L., Almeida, R. P., Coccioni, R., et al. (2016). The Barremian-Aptian boundary in the Poggio le Guaine core (central Italy): Evidence for magnetic polarity Chron M0r and oceanic anoxic event 1a. *Geological Society of America Special Paper*, *524*, 57–78. https://doi.org/10.1130/2016.2524(05)

Schlanger, S. O., & Jenkyns, H. C. (1976). Cretaceous oceanic anoxic events: Causes and consequences. *Geologie en Mijnbouw*, *55*, 179–184.

Selby, D., Mutterlose, J., & Condon, D. J. (2009). U-Pb and Re-Os Geochronology of the Aptian/Albian and Cenomanian/Turonian stage boundaries: Implications for timescale calibration, osmium isotope seawater composition and Re-Os systematics in organic-rich sediments. *Chemical Geology*, *265*(3–4), 394–409. https://doi.org/10.1016/j.chemgeo.2009.05.005

Taner, M. T. (1992). Attributes revisited. Technical Report, Rock Solid Images, Inc. https://rocksolidimages.com/pdf/attrib_revisited.htm

Tateo, F., Morandi, N., Nicolai, A., Ripepe, M., Coccioni, R., Galeotti, S., & Baudin, F. (2000). Orbital control on pelagic clay sedimentology: The case of late Albian "Amadeus Segment" (central Italy). *Bulletin de la Société géologique de France*, *171*(2), 217–228. https://doi.org/10.2113/171.2.217

Tejada, M. L. G., Suzuki, K., Kuroda, J., Coccioni, R., Mahoney, J. J., Ohkouchi, N., et al. (2009). Ontong Java Plateau eruption as a trigger for the early Aptian oceanic anoxic event. *Geology*, *37*(9), 855–858. https://doi.org/10.1130/g25763a.1

Thomson, D. J. (1982). Spectrum estimation and harmonic analysis. *Proceedings of the IEEE*, *70*(9), 1055–1096. https://doi.org/10.1109/proc.1982.12433

Trabucho Alexandre, J., Van Gilst, R. I., Rodríguez-López, J. P., & De Boer, P. L. (2011). The sedimentary expression of oceanic anoxic event 1b in the North Atlantic. *Sedimentology*, *58*(5), 1217–1246. https://doi.org/10.1111/j.1365-3091.2010.01202.x

Waltham, D. (2015). Milankovitch Period Uncertainties and Their Impact On Cyclostratigraphy. *Journal of Sedimentary Research*, *85*(8), 990–998. https://doi.org/10.2110/jsr.2015.66

Wang, C., Hu, X., Huang, Y., Scott, R. W., & Wagreich, M. (2009). Overview of Cretaceous Oceanic Red Beds (CORBs): A window on global oceanic and climate change. S. S. 91. *Cretaceous Oceanic Red Beds: Stratigraphy, Composition, Origins, and Paleoceanographic and Paleoclimatic Significance*, 13–33.

Wang, Y., Bodin, S., Blusztajn, J. S., Ullmann, C., & Nielsen, S. G. (2022). Orbitally paced global oceanic deoxygenation decoupled from volcanic CO2 emission during the middle Cretaceous Oceanic Anoxic Event 1b (Aptian-Albian transition). *Geology*, *50*(11), 1324–1328. https://doi.org/10.1130/G50553.1

Weissert, H. (1989). C-isotope stratigraphy, a monitor of paleoenvironmental change: A case study from the early cretaceous. *Surveys in Geophysics*, *10*, 1–61. https://doi.org/10.1007/BF01901664

Whitechurch, H., Montigny, R., Sevigny, J., Storey, M., & Salters, V. J. M. (1992). K–Ar and $^{40}Ar/^{39}Ar$ ages of central Kerguelen Plateau basalts. *Ocean Drill. Program Sci. Results*, *120*, 71–77.

Wu, H. C., Zhang, S., Hinnov, L. A., Jiang, G., Feng, Q., Li, H., & Yang, T. (2013). Time-calibrated Milankovitch cycles for the late Permian. *Nature Communications*, *4*(1), e2452. https://doi.org/10.1038/ncomms3452

Zhang, Y., Ogg, J. G., Minguez, D., Hounslow, M. W., Olaussen, S., Gradstein, F. M., & Esmeray-Senlet, S. (2021). Magnetostratigraphy of U-Pb–dated boreholes in Svalbard, Norway, implies that magnetochron M0r (a proposed Barremian-Aptian boundary marker) begins at 121.2 ± 0.4 Ma. *Geology*, *49*(6), 733–737. https://doi.org/10.1130/G48591.1